CHALMERS
UNIVERSITY OF TECHNOLOGY

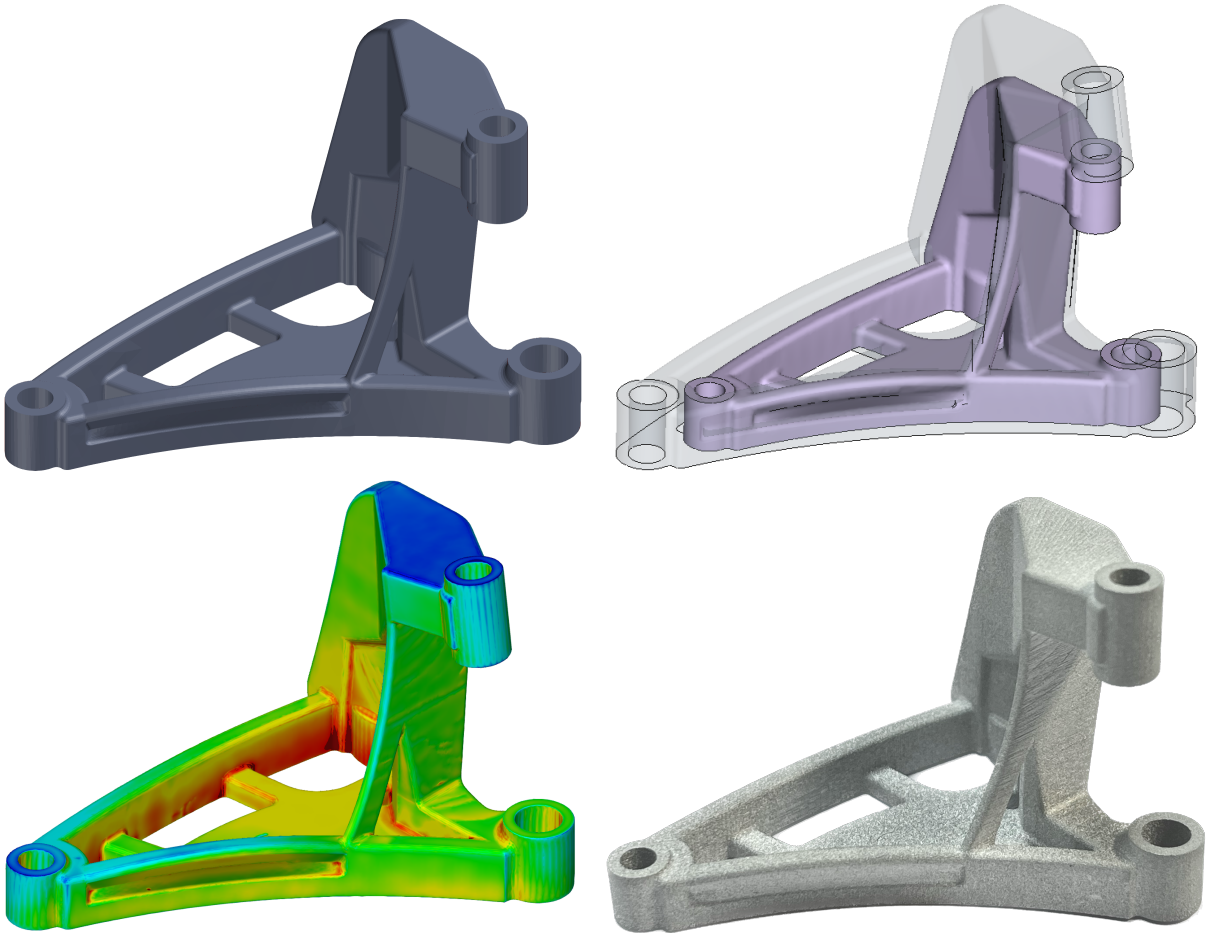

Product Design and Simulation for Metal Binder Jetting

An investigation of sintering deformation and design compensation in Simufact Additive

Master's thesis in Product Development

Simon Andersson & Garrett Dawson

Department of Industrial and Materials Science
CHALMERS UNIVERSITY OF TECHNOLOGY
Gothenburg, Sweden 2023
www.chalmers.se

Master's thesis 2023

Product Design and Simulation for Metal Binder Jetting

An investigation of sintering deformation and design compensation in Simufact Additive

Simon Andersson & Garrett Dawson

CHALMERS
UNIVERSITY OF TECHNOLOGY

Department of Industrial and Materials Science
Chalmers University of Technology
Gothenburg, Sweden 2023

Product Design and Simulation for Metal Binder Jetting
An investigation of sintering deformation and design compensation
in Simufact Additive
Simon Andersson & Garrett Dawson

Supervisor: Erik Adolfsson, RISE
Co-supervisor at Chalmers: Alberto Cabo Rios
Examiner: Eduard Hryha, Department of Industrial and Materials Science

Master's Thesis 2023
Department of Industrial and Materials Science
Chalmers University of Technology
SE-412 96 Gothenburg
Telephone +46 31 772 1000

Cover: A comparison of the CAD, simulation, scanned, and physical geometries of a component investigated during the thesis.

Typeset in LaTeX
Printed by Chalmers Reproservice
Gothenburg, Sweden 2023

Product Design and Simulation for Metal Binder Jetting
An investigation of sintering deformation and design compensation
in Simufact Additive
Simon Andersson & Garrett Dawson
Department of Industrial and Material Science
Chalmers University of Technology

Abstract

Metal Binder Jetting (MBJ) is an Additive Manufacturing (AM) method in which parts are built layer-by-layer using metal powder and a selectively deposited liquid bonding agent. MBJ can produce complex geometries with competitive physical properties. The as-printed part must undergo sintering to densify the component from ~50% to over 95% relative density and to achieve the desired physical properties. This densification corresponds to linear part shrinkage on the scale of 20% in addition to other deformations that may result from the high-temperature process. Shrinkage and deformation act as obstacles to creating parts with required geometrical tolerances when using MBJ.

Simulations of the sintering stage of the process present one possible way to improve geometry when addressing and compensating for shrinkage and deformation. The Simufact Additive Binder Jet module, developed by Hexagon AB, uses a finite element analysis (FEA) simulation of the sintering process and material model to predict the change of the geometry and the deviation from the desired tolerances. Additionally, there is the option to create a compensated, pre-deformed geometry that should sinter to the desired geometry based on the simulation results. This work has focused on investigating the sensitivity of input parameters of the simulations and the accuracy of simulation predictions compared to experimentally printed and sintered parts.

Investigation of simple 10mm cube geometries has shown that the Simufact simulations predict shrinkage on a similar scale to previous research but underestimate the shrinkage anisotropy in the build direction. When using the default material model, the pre-deformed geometry created by Simufact lead to an improvement in compliance with geometrical tolerances in 3 out of 5 tested geometries after sintering. An adjusted model applied to a complex geometry showed improved results from the default settings but with room for further improvement, indicating that adjusting simulation settings can improve simulation fidelity compared to real parts. Adjustments to the material model showed a more substantial influence on the results of simulation compared to adjustments in the sintering profile, with temperature notably showing little to no effect on predicted densification.

Keywords: additive manufacturing, metal binder jetting, Simufact Additive, sintering, shrinkage, deformation, simulation, design compensation.

Acknowledgements

The authors would like to extend our gratitude to those who have assisted and supported our work on this project.

Firstly, we would like to acknowledge the project examiner, Eduard Hryha, and the project supervisor, Erik Adolfsson, for their guidance throughout the thesis work.

We would like to express our thanks to RISE and AM Center staff for their support and for providing an encouraging environment in which to conduct our work. Also, extending special thanks to Ludiwg Eriksson for his assistance with printing & general matters, Martin Ohlsson for his assistance with simulations & Simufact Additive, and Lars-Olof Ingemarsson for his assistance with 3D scanning. Their reliable support was essential to the advancement of this thesis.

Additionally, we would like to acknowledge the advice and supervision provided by Alberto Cabo Rios and Erika Tunneskog for their guidance. Finally, we would like to thank Peter Hammersberg for his guidance and instruction with JMP and DOE.

The master thesis work was carried out at the Application Center for Additive Manufacturing at RISE, the Research Institutes of Sweden in collaboration with the Centre for Additive Manufacture – Metal at Chalmers University of Technology. Hexagon AB is also acknowledged for its support with regard to the software Simufact Additive Binder Jet Module.

Simon Andersson & Garrett Dawson, Gothenburg, June 2023

List of Acronyms

Below is the list of acronyms that have been used throughout this thesis listed in alphabetical order:

AM	Additive Manufacturing
CAD	Computer-Aided Design
DfAM	Design for Additive Manufacturing
DM	Digital Metal
DOE	Design of Experiments
FEA	Finite Element Analysis
HIP	Hot Isostatic Pressing
MBJ	Metal Binder Jetting
PSD	Particle Size Distribution
RQ	Research Question
SSS	Solid-State Sintering

Contents

List of Figures

List of Tables

1
Introduction

This chapter introduces the research work by providing a brief background into the topic as well as the aims and limitations of the investigation.

1.1 Background

This project was conducted at the Research Institute of Sweden (RISE) in the frame of the Center for Additive Manufacturing - Metal (CAM^2) coordinated by Chalmers University of Technology. The project focused on one of the growing additive manufacturing (AM) methods, specifically metal binder jetting (MBJ). In this process, a CAD file is printed by layers of metal powder being bonded together, and then this green part is processed and sintered [1]. During this process, the part shrinks which, together with the impact of external forces, e.g. gravity, friction to the substrate, etc., can cause nonuniform deformations that are difficult to predict [2, 3]. This project set out to investigate this shrinkage and deformation behavior in order to determine how accurately the simulation software from Hexagon AB, Simufact Additive, and its Metal Binder Jetting module, can be used to simulate and predict these deformations. Also, this work investigated whether the design can be altered to compensate for this.

On a societal level, this project could potentially contribute to improved simulations in AM and in turn its acceptance into industrial settings. By improving the capabilities of the technology its benefits, such as improved customization and more sustainable manufacturing closer to the customers, will become more accessible. This relatively new area of manufacturing can affect everything from manufacturing in industrial settings to the production of smaller parts and toys for use in people's homes. Currently, MBJ is not a fully understood process, thus it is not a widely adopted manufacturing method. This project acts as a step to improve MBJ reliability as a supplement to traditional manufacturing methods.

When it comes to relating to the ecological aspect of the project, UN sustainability goals 8, 9, and 12 are the most relevant as they relate to the development of sustainable industry, economic growth, and the responsible consumption and production of resources [4]. Additive manufacturing in general and MBJ can help with advancing these goals as they are methods that focus on developing less wasteful methods of manufacturing along with contributing to the increased ability of local development and manufacturing.

The ethical aspects of this project are rather limited as the project consists of an investigation into the reliability of software that is used to analyze the additive manufacturing method of MBJ. From a broader perspective, one could look into the concept of additive manufacturing and what kind of ethical aspects could be derived from that sector as a whole. One aspect that could be considered is that the process of additive manufacturing makes it easier to manufacture products locally and in-house because the process is much less space intensive and works quite well for many smaller components. Closer production would contribute to more local manufacturing jobs and would make the process of oversight into worker welfare easier, compared to having the manufacturing take place overseas in a factory with poor oversight.

This project aimed to investigate the Binder Jetting Module of Simufact Additive. The project host, RISE, was interested in determining the reliability and accuracy of the simulations compared to reality and wanted a better understanding of how the software can compensate for the designs. The work to address these aims was divided into 4 main areas: a literature study, design and process simulation, experimental work, and analysis. The literature study focused on the design and simulation processes for MBJ as well as previous research on sintering anisotropy in MBJ parts. The simulation stage used the Simufact Additive 2022 MBJ module (Hexagon AB) [5]. CAD models were created in either Catia V5 or Fusion 360. The experiments included printing geometries with RISE's MBJ printer and using a digital scanner to measure the deformations at different stages of the process. Some parameters under investigation included part size, geometrical features, and material properties. The analysis consisted of a sensitivity analysis of the different input and output parameters that were used in the simulation, conducted with the help of the statistical software JMP.

1.2 Limitations

The project was carried out over 20 weeks creating some limitations on the scope of the project. Also, there were some limitations related to the availability of equipment. RISE uses an on-site Digital Metal DM P2500 printer; other printer models were not used during the project. Only one print material is investigated, 316L stainless steel produced by Höganäs AB, so the variation in the behavior of other materials is not included in this project. The printer and sintering settings were not adjusted between prints so the only variation was the geometry provided and the random minor variations that occur during printing.

1.3 Specification of the Issue under Investigation

The following are specific research questions (RQ) that were addressed during the project relating to the primary objectives set out at the beginning of the project.

1. How well can the simulation tool predict the deformation of parts after sintering?

2. Can the prediction be used to redesign the original geometry to compensate for the deformation?
3. To what extent do different parameters influence the outcome of the simulation?

With regards to RQ1, the investigation considered the overall accuracy as well as relevant parameters included in the model. Included in this was determining a way to effectively compare physical geometries with their simulated counterparts. RQ2 pertains mainly to the Compensation Optimization tool included in the software, but also considers how well the simulations results can be interpreted by the user to identify where the part requires redesigning. RQ3 includes parameters that act as inputs for the simulation such as the sintering profile in terms of time and temperature, part orientation, as well as geometrical factors like the part size and features such as holes, fillets, overhangs, etc.

1.4 Methodology

The process of investigating the reliability of Simufact Additive was divided into several steps, as mentioned before. The investigation began with a literature study pertaining to the state of the science regarding MBJ. This initial research formed the basis of the early design of the phase 1 components that were manufactured and tested. After the design phase, components were exported into Simufact Additive for initial analysis. The components were then converted into a printable format and exported to the on-site MBJ printer. After the components had been printed and sintered, they were scanned with a GOM scanner to digitize the geometry to compare to the original CAD geometry. Sintering is the process stage in which the majority of deformation occurs and is the area of most interest in this research. After manufacturing, sintering, and scanning MBJ parts, the geometries were compared with results from Simufact simulations. The methodology is further expanded upon in Chapter 3.

2
Theory

A short introduction of the additive manufacturing technology used - metal binder jetting - along with a description of the physical phenomena related to the printing and sintering processes.

2.1 Introduction to Metal Binder Jetting

The area of modern Additive manufacturing (AM) includes a range of technologies formally defined in ISO 52900 as a "process of joining materials to make parts from 3D model data, usually layer upon layer, as opposed to subtractive manufacturing and formative manufacturing methodologies" [1]. Recent decades have seen an explosion of interest in the various metal AM methods and their potential applications, both from the scientific community and industry [6]. One of the variations of AM is the method called Metal Binder Jetting (MBJ), which is an AM process in which a "liquid bonding agent is selectively deposited to join powder materials" [1]. MBJ is the AM process relevant to this thesis.

The MBJ process consists of five main steps [7]:

1. The printing on the powder bed using metal powder, and a liquid binder which weakly bonds the metal powder until the next step of the process
2. Curing of the part in a relatively low-temperature oven
3. Removing the unbound powder in the powder cake around the cured part (depowdering)
4. Debinding and sintering of the part to improve the strength
5. Post-processing of the part if needed, depending on the application of the part

The initial printing of the part takes place within a sealed chamber to prevent the fine metal powder from escaping the manufacturing area [7]. Inside this chamber is a build plate on which the metal powder is deposited. Then the binder is selectively dropped on top of the powder that is spread out upon the previously binder-deposited layer. This deposition and binding continue in a layer-by-layer process, until the bound part has reached the shape of the 3D design file that was imported into the machine. A schematic of the printing chamber along with descriptions of the different parts and their function can be seen in Figure 2.1. After the formation of the part, the next step is to put the printed part in an oven to cure it. This process usually reaches a temperature of around 200 °C and evaporates the solvent carried from the binder.

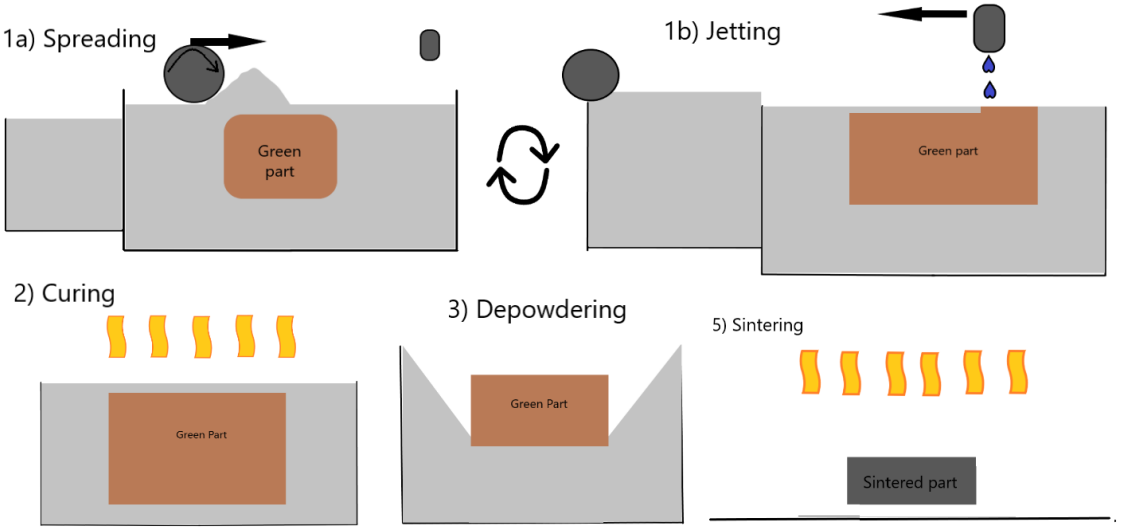

Figure 2.1: This schematic illustrates the MBJ process including the printing of the parts on the powder bed; different parts of the printer and their purpose; and the curing, debinding, and sintering of the part.

After the completion of the curing stage, the excess power around the cured part will need to be removed [2]. This is performed inside a depowdering chamber which is a sealed box with a window and internal gloves that are used to handle the part inside of the box. At this stage, the part has poor mechanical properties and is very brittle and fragile. To transition from this low-density and brittle state to the part with desired mechanical properties, the part is sintered. The sintering process consists of putting the cleaned parts into a high-temperature sintering furnace under a protective atmosphere or vacuum for several hours at high temperatures. The initial debinding burns away the binder that remains within the structure and the sintering densifies the part to a density above 90%, depending on the sintering profile applied as well as the material composition. This sintering process drastically increases the mechanical performance of the part.
Removing the binder and densifying the part results in linear shrinkages on the scale of about 20% [7]. The amount of shrinkage varies depending on various characteristics such as the green part density and sintering parameters, such as time and temperature. This shrinkage is not uniform and can cause distortions in the final part's geometry and mechanical properties [2]. Previous studies show similar sintering shrinkage measured in the recoater and nozzle movement directions, and more substantial shrinkage is observed in the build direction [8, 9, 10]. These actions are generally in orthogonal directions which can lead to anisotropy in the printed part, for example, non-homogeneous porosity distribution.

2.1.1 Proper Selection of Metal AM

Looking at the current generation of metal AM as a whole, and MBJ more specifically, what are the significant advantages of the technology and what should it be

applied to take the greatest benefit of its unique properties? The field of AM has found its special niche in the low-volume production and geometrically complex components that place a high value on weight reduction and the ability to customize components for a specific purpose [11]. These features have translated well into the areas of on-demand, low-cost rapid prototyping, local production of low-volume components, and the ability to compensate for risk in supply chains.

One of the main applications of AM is in the manufacturing of functional prototypes [12]. These prototypes can usually be produced at a fraction of the time and cost that would take with traditional manufacturing methods and it enables faster evaluation and adjustment cycles while developing or improving products.

Another area in which metal AM can be used to its full potential is in the local, low-volume production of custom components [12]. With traditional manufacturing, this type of production often has a prohibitively high startup cost and is often disregarded in favor of importing ready-made components instead. AM provides a cheaper initial cost than most traditional manufacturing and the production can more easily be altered to accommodate alterations in the specifications of the production. Examples of industries where this more localized production could be utilized are the manufacturing of medical and dental components or spare parts for cars, homes, or general appliances. These are all areas in which each request for a component of the part will be slightly unique and the cost of providing storage from all the possible combinations of components can be a large obstacle to the financial stability of the company providing the product.

Other large industries where metal AM has huge potential are the automotive, aerospace, defense, communication, energy, and industrial tooling sectors [12]. The main benefits of applying AM in these industries are the potential for weight reduction and the ability to manufacture geometries that are impossible or prohibitively expensive using more traditional manufacturing methods.

Beyond the economic benefits that metal AM can provide, there is also a potential for positive environmental and social impact that can follow the appropriate implementation of this manufacturing method [13]. The largest environmental impact that the wider implementation of metal AM could achieve is the reduction of the need for transporting components over waste distances and instead producing them locally. The social upside of this would be an increase in local production and job opportunities, while also contributing to a decrease in CO_2 impact from the transportation of these components.

The main benefit of using specifically MBJ printing is that it is a "cold" process [14]. This means that heating is not required during the printing process to melt the powder. This leads to the removal of the need for a protective atmosphere while printing and it also removes high-powered components such as lasers or electron beam generators that are needed in some "hot" printing processes. Another benefit of having a "cold" process is the avoidance of temperature gradient during printing which can cause distortions in the print [15].

2.1.2 Challenges of Industrial Utilization of MBJ

As mentioned previously AM technology has the potential to improve certain sectors of the manufacturing industry and can lead to reduced lead time and faster concept generations. There are, however, some critical challenges for this technology that must be taken into consideration if it is to be successfully implemented.

These challenges mainly relate to AM specializing in low production volume, high variability, and geometrically complex components [12]. High precision with complex features comes at the expense of manufacturing speed when dealing with high production volume. Conventional manufacturing methods are substantially better at producing a high volume of parts and processing more material at once; this is especially true when dealing with components with low complexity and low variability. Another factor that proves challenging for current metal AM technology is the relatively limited selection of materials that are accessible for AM compared to traditional manufacturing. This is also related to the manufacturing of the metal powder that is used in metal AM and requires an extensive production system on its own.

The last challenges relate to the relative immaturity of the field of AM [12]. This means that the manufacturing technology lacks universal understanding and acceptance in the industry which has limited its implementation. This lack of universally accepted implementation translates into a lack of standardization and a limited understanding of what qualifications are needed for different applications of metal AM in the industry. Along with this, the technology has not yet had time to fully integrate into the current industrial setting, resulting in the unfulfilled potential for combining metal AM and traditional manufacturing methods.

In conclusion, AM and MBJ, like all manufacturing technologies have their limitations. These limitations will need to be well understood in order to efficiently and effectively integrate these technologies into the existing production chain. Understanding the area of design for AM is something in particular that will need to be developed further as it is currently lacking in the industry. The AM technology is not aiming for and will never be able to substitute traditional manufacturing methods in the manufacturing industry. It is however capable to assist with the manufacturing of geometrically complex components with a high degree of customization.

2.2 Sintering - Shrinkage, and Deformation

Sintering is a necessary processing step for MBJ to create the final part with appropriate physical properties [7, 16]. The debinding process removes most of the binder from the green part and the resulting 'brown' part is sintered in a furnace [17]. Sintering can be defined as a thermal treatment that bonds particles together into a single solid structure via mass transport mechanisms at an atomic scale [10, 18]. There are several sintering processes for metals that vary depending on the phases present in the material during sintering, including solid-state sintering (SSS), liquid phase sintering, and supersolidus liquid phase sintering [9, 10]. Generally 316L steel

is sintered without the presence of a liquid phase, so SSS is the only sintering process considered in this thesis.

Sintering densification in SSS is driven by the reduction of the system energy due to a reduction in the surface area [10, 18, 19]. The mass transport mechanisms are surface transport (surface diffusion and evaporation-condensation) and bulk transport mechanisms (grain boundary diffusion, plastic flow, viscous flow, and volume diffusion), where the bulk transport mechanisms contribute most strongly to the overall densification of the part [18, 19]; see Figure 2.2. Sintering densification is improved in processes with small particles, longer sintering times, and higher sintering temperatures [19]. Additionally, sintering is often performed in the presence of a controlled atmosphere or vacuum to prevent potentially detrimental reactions with oxygen in the atmosphere such as oxidation [10]. These reactions impede the sintering process so protective atmospheres, which generally use inert or reducing gases, are used. When sintering with 316L, a H_2 or Ar-H_2 atmosphere is common to reduce surface oxides.

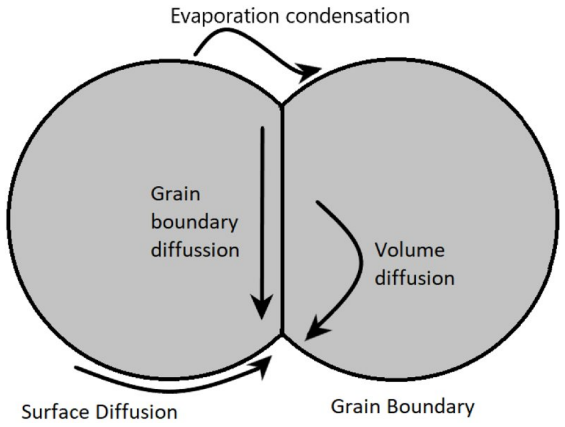

Figure 2.2: Depiction of sintering mass-transport paths, redrawn from [9, 18]

While sintering improves the material properties, it also causes significant shrinkage and potential deformation of MBJ parts. A sintered part transitioning from approximately 50% density to over 95% density corresponds to linear shrinkage on the scale of 20% [3, 7]. While smaller magnitude shrinkage may occur during other stages of the processing, such as debinding, the vast majority of shrinkage occurs during sintering, and it is also the most likely stage for deformation or cracking and failure [2]. Small amounts of shrinkage may also occur if the part undergoes hot isostatic pressing (HIP) treatment, in which the part goes from ~95% density up to full density.

Sintering shrinkage and deformation can be accounted for via a trial-and-error design process, but being able to predict and compensate before printing is more desirable [3]. Previous research has investigated parameters that tend to have the most effect on shrinkage and deformation:

- Powder distribution and green part density [3, 20]

- Print orientation and build direction [3, 8]
- Gravity [2, 3, 7, 20]
- Friction with build plate [3, 20]
- Sintering conditions [3, 8, 10, 17]

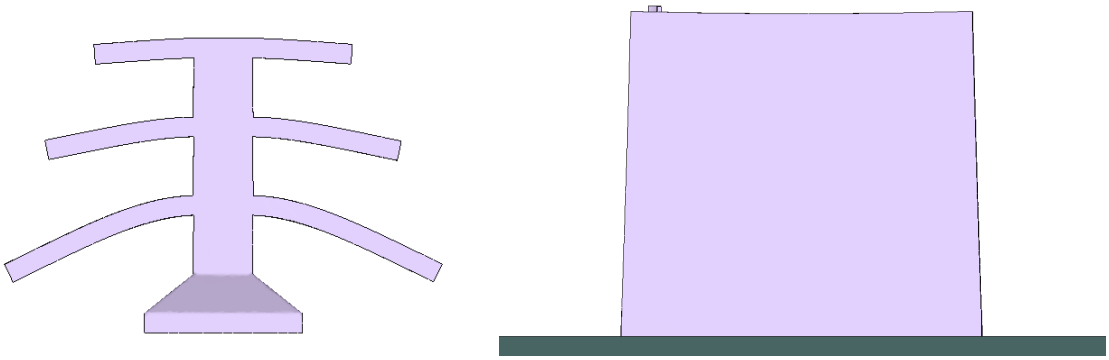

Figure 2.3: Examples of sagging and frictional deformations shown at one and four times scaling respectively. Taken from results of Simufact Additive simulations.

The shrinkages during sintering are related to the characteristics of the printed parts. The denser the part is prior to the sintering stage, (i.e. high green part density) the less shrinkage will occur [20]. Additionally, a print will ideally have uniform density, or alternatively thinking uniform porosity distribution, throughout the green part to achieve a uniform sintered density [3, 20].

There are several factors in the printing process that can have an impact on the green part density: the properties of the powder, the recoater depositing the powder, and the liquid binder used to bond the particles together. The powder properties with the largest impact on the green density are the combination of the powder particle shape and sizes [21, 22]. This particle size distribution and shape will affect the packing density of each deposited layer. To achieve the highest packing density there should be a bimodal powder mixture, where there are small particles present to fill the gaps created by the larger, coarser particles [23]. Another factor contributing to a high powder bed density is the packing effect from recoating when each new layer is deposited [22]. In addition to the compaction effect from the recoater, the powder flowability also contributes to packing density. Finer powder allows for smoother and denser powder layers. Aside from the powder particle size and shape, binder saturation and penetration of the powder layer also contributes to the green density of parts [14]. To achieve the highest green part density, the binder distribution will need to be analyzed in combination with each individual material used in tandem with layer thickness and particle sizes, and shapes.

Anisotropic shrinkage in the build direction results from both the debinding and sintering stages. The shrinkage measured in the build direction, or the z-direction, generally exceeds the shrinkage in the x or y-directions [3, 8]. Gravity also can create deformations in the part during sintering when the heated metal becomes soft enough that the part can begin to sag due to its own weight [2, 3, 7, 20]. This applies to features such as overhangs as well, where unsupported areas may experience critical

vertical deformations. Additionally, gravity-causing particle rearrangement during sintering will lead to greater shrinkage in the build direction [9]. Non-homogeneous density or porosity distributions within the part, as well as lower rigidity of the powder compact along the build direction, are also major contributors to sintering anisotropy.

The movement caused by the shrinking part creates friction between the part and the baseplate and can contribute to additional deformations [3, 20]; see Figure 2.3. Some methods to counteract this already exist such as using a setter, or sintering support, made of the same material so that it will also shrink at the same rate as the part, which is available in some simulations. Also in the design stage, the designer should be aware of the weight of the part since the normal force is proportional to the frictional force.

Sintering parameters have been shown to affect both the shrinkage [3, 8, 17], final density [10], as well as the microstructure formation [3, 9, 18]. The sintering parameters of interest include heating rate, sintering temperature, and holding time at the sintering temperature [17].

2.3 Simufact Additive Software

Ideally, the deformation can be predicted and compensated for prior to printing using analysis software. This research uses the Hexagon software Simufact Additive, specifically the 2022 Metal Binder Jetting module, to analyze the MBJ prints and to gauge the efficacy of the software. The program is optimized for stainless steel 316L and accounts for several phenomena during the simulation including diffusion, gravity, friction, creep, and grain growth [20]. The software uses a finite element analysis (FEA) simulation using component geometry, sintering orientation, supports and setters, and process and material parameters as input.

In line with demand from the industry, the Simufact Additive can perform deformation compensation based on the inputs given [5, 20]. It is an iterative FEA simulation resulting in a pre-deformed part that should have the desired dimensions after sintering. While the predictions are not perfect, dimensional accuracy of up to 95% has been reported with some calibration efforts [20]. Results also vary depending on factors like part geometry, and powder quality. The software includes a distortion compensation tool [24], which will be featured in this research. An example is given in Figure 2.4.

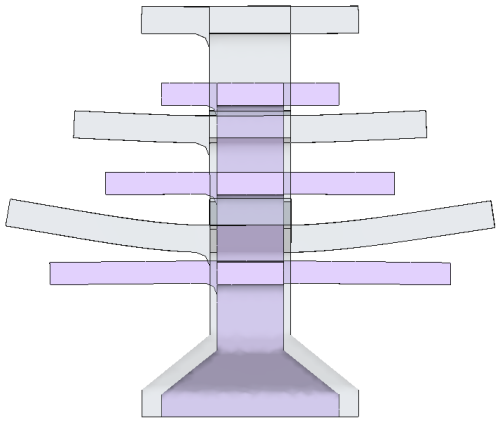

Figure 2.4: An example of the compensated geometry that Simufact additive can produce based on the expected shrinkage and deformation of the part. The shaded part is the compensated geometry based on previous calculations of the sintering deformation.

To begin the simulation, the software takes the geometry in the form of a .step or .stl file and loads it into the workspace [24]. The user chooses a material to assign to the geometry and can provide values for the sintering process including initial relative density and sintering thermal route. The selection of material and sintering parameters are of high significance as they will greatly affect the output of the simulation, in the form of sagging, shrinkage, and final density. If the selected values do not match the real-life process that will be implemented, the results from the simulation will be of low value. This necessitates a thorough understanding of both the sintering process and the material that will be simulated using the software.

The material data is available in a material library, or a custom material can be added to the library. When using the deformation compensation, the user may set either an acceptable distortion as a convergence goal or a maximum number of iterations to determine the end of the simulation iterations. Simufact is then able to measure the deviation between a sintered part and a reference geometry [5]. When the simulation is completed and the distortion compensation has reached the convergence goal set, the compensated geometry can be directly exported as a .stl file. There is also the possibility to export the geometry from the software during timed increments of the simulation.

3
Methods

This chapter describes the methodology of the project. It contains a description of the literature study, the geometry selection, simulation software, the equipment used, and the data analysis methods.

3.1 Literature Study

MBJ is a technology experiencing constant development. The technical terms and standards within AM tend to change over just a few years, which became a limiting factor in the initial literature study. The practical consequence of the rapid development of MBJ is that information becomes outdated faster than other topics. The initial literature study consisted of thorough searches through the Chalmers Library and Google Scholar. This search was mainly focused on articles, papers, and literature published in the areas of MBJ, Sintering, and Simufact prioritizing literature published more recently.

3.2 Geometry Selection

A variety of geometries were used in the simulations and for manufacturing components. These geometries ranged from simpler shapes such as cubes, cylinders, and rectangles, to more complex shapes such as I-beams, T-beams, and cross shapes. Later stages of the project used more complicated geometries with features of interest - e.g. holes, fillets, overhangs, etc. - that would be used for simulations using the Compensation Optimization tool. Finally, a part with complex geometry was chosen to investigate how a complex part would perform in the simulation and how accurately the deformation compensation can be performed. While good performance with simpler geometries is important, to be useful in industry settings Simufact Additive should also accurately simulate complex geometries.

Simpler geometries were used to be able to more accurately differentiate how different geometrical parameters influence the accuracy of the results of the Simufact simulation. Initially, phase 1 geometries in the form of cylinders and cubes were used to gauge how changing a single parameter - e.g. height, diameter, etc. - would influence results. These geometries were also simulated without performing geometrical compensation to establish a baseline for the reliability of the software to predict unaltered sintering deformation. These predictions pertained to the geometries simulated final density, sagging, and shrinkage in the x-, y- and z-directions.

Pre-deformed geometries were analyzed in the following stage of the study.

The intermediate stages of the project investigated geometries that resembled parts that were designed to include features that can face difficulties in AM including angled surfaces, holes, bridges, fillets, and overhangs. After reviewing and refining the concepts, a total of five potential candidates remained. The phase 2 geometries were modeled in Fusion 360 can be seen in Figure 3.1.

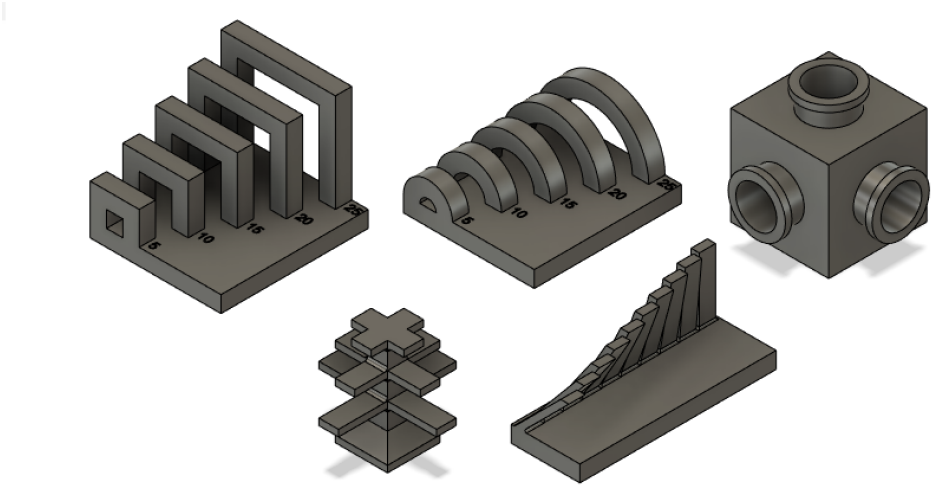

Figure 3.1: CAD images of phase 2 geometries from Fusion 360.

In the last stages of the project, the investigation focused on a geometry considered complicated enough to equate to what could be considered a well-toleranced engineering part in an industrial setting. It includes an overhang, thin walls, holes, and support similar to an arch. This phase 3 geometry was designed and provided by RISE staff. The simulation and compensation of this geometry served as the final assessment of the Simufact Additive Binder Jet module's capability to predict and compensate for sintering deformation within the context of this project. A CAD image of the phase 3 geometry visualized in Fusion 360 is shown in Figure 3.2.

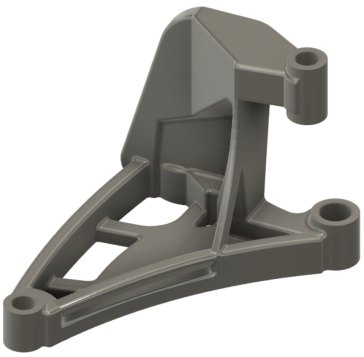

Figure 3.2: A CAD image of the phase 3 geometry from Fusion 360.

3.3 Simulation

The purpose of using increasingly complex geometries was to incrementally test the reliability of Simufact Additive. Specifically the 2022 Metal Binder Jetting module, in terms of accurately predicting the deformation of the geometry that will occur during sintering and see if the software can compensate for said deformation. The goal of this testing was to find out if the Simufact Additive scaling prediction is superior to Digital Metals' provided scaling factor, which is about 1.2 in the x, y, and z-direction. The initial simulations also served as trial-and-error sessions for learning the program and the optimal approach to setting up the simulations including considerations of running multiple simulations with different parts or having one large simulation with multiple parts on the same build plate. The majority of the simulations performed the calculations with a single component at a time to decrease the simulation time.

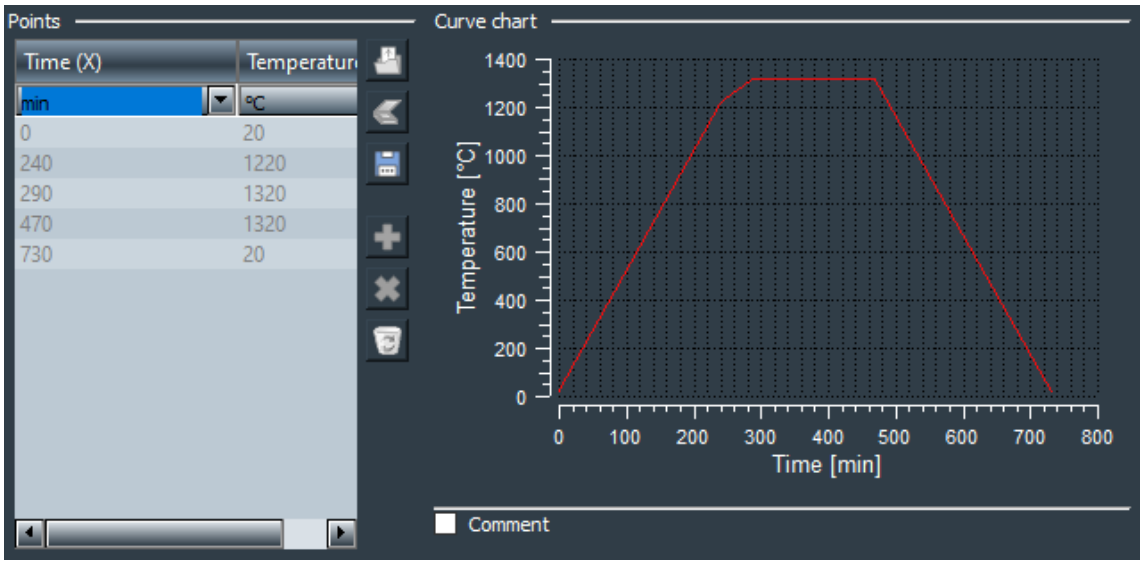

Figure 3.3: The parameters used for the sintering of the artifacts in the simulation in Simufact are visualized as numbers and as a graph as shown in the software interface. These values and times were based on the sintering parameters used at RISE during the sintering of the printed components.

A template with the simulation settings, material parameters, and sintering details was used to maintain consistency across the simulations. This template was kept unmodified for the initial simulations but later altered in the sensitivity analysis performed in JMP [25]. The sintering profile was selected based on discussions with relevant personnel at RISE and is shown in Figure 3.3 and the default friction coefficient, 0.3, was used. This friction coefficient affects the friction between the part in the sintering substrate at the bottom of the substrate. Increased friction can lead to distortion similar to that shown with the cube in Figure 2.3. The initial green part density was originally set to 53%, this number was however updated in later simulations based on measurements taken of the printed geometry. These values

and times for the simulations were based on the real-life sintering parameters used at RISE during the sintering of the printed components. The acceptable distortion used varied depending on the total size of the geometry under consideration and the mesh size used, with the goal to restrict computational costs to a reasonable amount while still requiring several iterations to converge. The MUMPS Parallel Direct solver was used for these simulations. The standard material 316L Stainless Steel from the Simufact Additive material database was used in most of the simulations and only altered later in the project when different material parameters were under investigation.

3.4 Experimental Procedure

The creation and analysis of the components used in this paper required several advanced machines. The mentioned hardware along with the knowledge of how to operate these machines was derived from technicians with expertise operating the specific machines, both at RISE and at Chalmers.

3.4.1 Printing and Sintering

All parts manufactured in the project were printed at the RISE laboratory in Mölndal using the Digital Metal (DM) P2500 using DM 316L stainless steel powder. The settings that were used during the prints can be seen in Appendix A.1. The powder is sieved with Retsch (Germany) 45 and 32-micron sieves and then mixed in a Turbula mixer (Wab-group) to evenly distribute the powder. The powder size distribution (PSD) was measured using a Mastersizer 3000 (Malvern, United Kingdom).

The curing of the parts was performed at 200°C and the dwell time depended on the building height in the build box. The cured parts are depowdered manually in an MDS 1000 depowdering machine. The setting for the debinding was as follows: heating at 3°C/min to 345°C, followed by 2 hours holding time and cooling at 5°C/min to 20°C. The standard setting for the sintering was as follows: heating to 1250°C with a heating rate of 5°C/min, then with a slower heating rate of 2°C/min to a sintering temperature of 1320 °C followed by 3 hours holding time, and further cooling to room temperature with a cooling rate of 5°C/min.

In addition to the standard sintering of the geometries, one sintering cycle was performed using dilatometry on one of the phase 1 geometry 10mm cubes. This dilatometry measures the dimensional variation of the cube as it is sintered. This method also measures the time and temperature of the sintering process so that the gathered data can be plotted and compared to other sintered or simulated samples. The machine that was used while performing the sintering of the cube was a vacuum-tight dilatometer DIL 402C from NETZSCH (NETZSCH-Gerätebau GmbH, Germany) equipped with a W-Re thermocouple for inert or reducing atmosphere. The methodology for using this machine was inspired by the paper from Alberto Cabo Rios et al. [10].

3.4.2 Physical Measurements

The physical specimens were measured to compare to simulated geometries. Measurements of phase 1 geometries were conducted with calipers with .001 mm precision and a high precision scale with 0.0001 g precision for geometries under 200g and a 1g precision scale for geometries above 200g. In addition to the manual measurements, the parts were scanned with an ATOS III triple scanner (GOM, Germany) with a resolution of up to 0.01 mm. The scanner operation followed the instructions in the *ATOS User Manual Hardware ATOS III Triple Scan - Rev. 02* manual. The scanned geometries were compared to the original virtual geometry using GOM Inspect software. GOM Inspect can report surface deviations, simple distance measurements, and volume measurements. The GOM software was used in accordance with the *Inspection Basic GOM Software 2018 3D Metrology* handbook, provided by GOM. No surface treatment was performed on either green or sintered parts, as such the surfaces of the green and sintered parts are relatively rough. This may lead to a slight overestimate of the length measurements of the parts when using calipers or similar tools.

Measurements were taken both on the green bodies after depowdering and the final parts after the sintering stage. This is an essential step so that deformations or errors resulting from the printing and curing stages are not incorrectly attributed to the sintering. Additionally, volume measurements from GOM Inspect and mass measurements were used to estimate the uniform green density after depowdering and relative density after the sintering of the parts.

3.5 Parameter Study

One of the points of interest in this project was the investigation of the impact that the different sintering parameters had on the shape and properties of the final geometry. The geometry that was used for this analysis was a relatively simple "tree shape" that was designed and provided by Alberto Cabo Rios at Chalmers. This tree was deemed to have the necessary features to measure the sagging and shrinkage and compare them with Simufact Additive simulations. The initial shape of the tree is shown in Figure 3.4.

The default 316L powder included in the material library was used. The grain size was the only material parameter that varied at this stage. Other material parameters such as the activation energy of viscous flow and a pre-exponential constant were altered in a parameter study that took place later in the project. The initial grain size in this first parameter study is assumed to be the same as the D50 statistical distribution of particle sizes in the powder used for the printing of the parts. Table 3.1 shows the parameters investigated.

When analyzing the sintering parameters of the MBJ sintering module in Simufact Additive software, a total of five continuous input parameters were chosen. These included the green part's relative density (initial density), the sintering temperature defined in the software as the max holding temperature in the sintering furnace,

Parameter	**Range**
Max Temp (°C)	1210 - 1370
Temperature Ramp Rate (K/min)	2 - 10
Holding Time (hr)	1 - 6
Initial Green Density (%)	50 - 65
Grain Size (Powder particle size) (µm)	5 - 45

Table 3.1: List of parameters included in the investigation.

the ramp rate for the temperature in the furnace, the median powder particle size (D50, referred to as grain size of the powder), and the holding time at the maximum temperature in the sintering furnace. These parameters were included in the analysis as they are the input parameters that can be changed in the interface of the software without altering the material model. The outputs or responses in the experiments were determined to be shrinkage in the x, y, and z-directions, along with final density and sagging on the longest of the arms.

The maximum temperature was of interest because of its strong impact on densification [10, 18, 19]. Sintering at too high temperatures can lead to partial melting and loss of shape, and at too low temperatures and the part will not densify to the extent required. The melting point of 316L stainless steel is 1400 °C in the Simufact Material Library accompanying the Simufact Additive software, so the temperatures used in the simulations were below that. The ramp rate is also of interest for densification [5]. Experimentally, the ramp rate must be slow enough that the temperature within the component is relatively uniform so that the densification is uniform. However, a high ramp rate would be desirable to reduce the total time needed for sintering. Similarly, the holding time at the maximum temperature affects densification and process time.

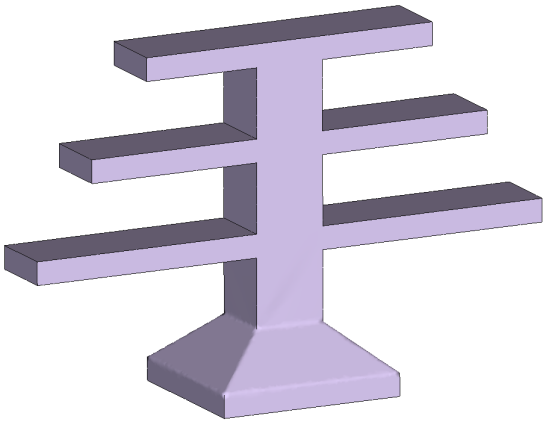

Figure 3.4: CAD representation of tree geometry used in the parameter study.

As mentioned earlier in the theory section, the initial green density is highly correlated to the part shrinkage. There is some variability in green density depending

on the printing process and material parameters, so it is of interest to know how an increase or decrease in green density will affect the sintered part. Grain size, or powder particle size, is also of interest because of the impact that it will have on the ability of the part to be printed correctly and to densify properly during the sintering stage.

The measurement tool within Simufact Additive was used to measure the linear shrinkage in the x, y, and z-directions of the component. Additionally, the sagging of the arms from the base of the tree was measured as a way of assessing the non-shrinkage deformation. Simufact Additive also created the final density distribution in the results module.

To robustly investigate this, Design of Experiments (DOE), specifically a definitive screening design using the DOE software JMP [25], was used. Within JMP one can insert the desired inputs factors and ranges, along with outputs and whether they should be maximized, minimized, or reach a target value. After inputting these simulation variables JMP will provide a matrix with several combinations of the intervals derived from the ranges of the settings. These settings will be combined in such a manner as to most effectively cover the response surface of the problem in the fewest experiments possible. The DOE table is given in Appendix B.1. The experiments with the parameters specified by the DOE were run in Simufact Additive, and the results were recorded in the same data table in JMP. From this table, JMP is able to perform several analyses including creating a statistical model or a factor screening to determine the influence of each individual input factor or a combination of factors.

4

Results

This chapter outlines the data and results gathered from the research performed. The results include a sensitivity analysis of parameters from the simulation, as well as measurements and insights from printed artifacts.

All printing, sintering, and scanning were conducted on-site at RISE with consistent process parameters and methodology outlined in Section 3.4.1. The dilatometry measurements were collected at Chalmers University of Technology.

4.1 Parameter Study and Sensitivity Analysis

The initial screening design was conducted using JMP [25] using the suggested 17 runs, later augmented to 25 runs in total. The full data spreadsheet can be seen in Appendix B.1. JMP provided the suggested input values for the given parameters which were then used in the simulations in Simufact. The results for final density; x, y, z-deformation; and the sagging of the tree arms were inserted into JMP to continue with the analysis.

The primary area of interest from this stage of the investigation was to determine to what extent each input factor influences any given output response. The factors considered in this stage are those which could be measured or changed within the current manufacturing process. Using JMP [25], a two-level screening tool was used to identify which factors and higher-order factor interactions have a significant impact on the responses. From this, a least squares fit model of the responses was created and the weighted importance of each factor was extracted. Figure 4.1 shows the importance of each factor for each response of the overall model.

These values display some clear patterns from the model to draw conclusions. Firstly, the initial grain size (D50) has the greatest effect on the overall model, and the strongest influence on the final density and sagging responses. Initial density influenced the shrinkage in all directions the most but also had a negligible effect on the sagging response. Notably, the maximum temperature during the sintering cycle was shown to have a practically negligible effect on all responses investigated.

Overall

Column	Main Effect	Total Effect
Grain Size	0.361	0.385
Initial Dens	0.28	0.293
Holding Time	0.165	0.188
Ramp Rate	0.127	0.143
Max Temp	0.002	0.003

Final Density

Column	Main Effect	Total Effect
Grain Size	0.505	0.53
Ramp Rate	0.206	0.222
Holding Time	0.192	0.215
Initial Dens	0.028	0.041
Max Temp	0.002	0.004

Sagging

Column	Main Effect	Total Effect
Grain Size	0.555	0.573
Holding Time	0.347	0.367
Ramp Rate	0.048	0.062
Max Temp	0.003	0.004
Initial Dens	0.001	0.002

Shrinkage X

Column	Main Effect	Total Effect
Initial Dens	0.461	0.478
Grain Size	0.228	0.252
Ramp Rate	0.136	0.152
Holding Time	0.103	0.127
Max Temp	0.001	0.002

Shrinkage Y

Column	Main Effect	Total Effect
Initial Dens	0.465	0.482
Grain Size	0.286	0.311
Ramp Rate	0.103	0.119
Holding Time	0.074	0.098
Max Temp	0.001	0.001

Shrinkage Z

Column	Main Effect	Total Effect
Initial Dens	0.443	0.46
Grain Size	0.232	0.257
Ramp Rate	0.144	0.16
Holding Time	0.107	0.131
Max Temp	0.001	0.002

Figure 4.1: Factor weights for Simufact input parameters and relevant output responses.

Source	Logworth	PValue	
Grain Size(5,45)	4.826	0.00001	
Ramp Rate(2,10)	4.681	0.00002	
Holding Time(1,6)	4.439	0.00004	
Grain Size*Ramp Rate	3.957	0.00011	
Holding Time*Ramp Rate	3.493	0.00032	
Max Temp(1210,1370)	3.295	0.00051	
Grain Size*Grain Size*Holding Time	3.292	0.00051	
Grain Size*Holding Time*Ramp Rate	2.985	0.00103	
Ramp Rate*Max Temp	2.899	0.00126	
Grain Size*Holding Time	2.692	0.00203	^
Holding Time*Max Temp	2.530	0.00295	
Holding Time*Holding Time	2.504	0.00313	
Initial Dens(50,65)	1.931	0.01173	
Holding Time*Initial Dens	1.903	0.01249	
Grain Size*Grain Size	1.819	0.01517	^
Ramp Rate*Ramp Rate	1.744	0.01803	
Max Temp*Initial Dens	1.354	0.04427	
Grain Size*Max Temp	1.302	0.04988	
Grain Size*Initial Dens	1.074	0.08441	
Grain Size*Holding Time*Holding Time	0.529	0.29603	
Ramp Rate*Initial Dens	0.355	0.44136	
Max Temp*Max Temp	0.069	0.85356	

Remove Add Edit ☐ FDR ('^' denotes effects with containing effects above them)

Source	Logworth	PValue	
Grain Size(5,45)	15.194	0.00000	
Grain Size*Ramp Rate	7.562	0.00000	
Holding Time(1,6)	7.445	0.00000	
Ramp Rate(2,10)	5.782	0.00000	^
Grain Size*Grain Size*Holding Time	4.251	0.00006	
Holding Time*Ramp Rate	4.005	0.00010	
Grain Size*Grain Size	3.113	0.00077	^
Grain Size*Holding Time	0.272	0.53404	^

Remove Add Edit Undo ☐ FDR ('^' denotes effects with containing effects above them)

Figure 4.2: Statistical weighting and significance of simulation parameters for the sagging response. The blue line represents the threshold for significance. The top graph considers many higher-order interactions while the lower graph only includes the significant factors.

The initial DOE was augmented with additional runs with the intention to more closely investigate the higher-order interactions between the factors in the model. Specifically, after initially finding that temperature was having a negligible effect on the responses, it was of interest to see if the temperature had an effect on the model in a higher-order interaction, such as a cross with holding time. Figure 4.2 shows the effect summary for the final density. Many interactions were included and the ones that did not meet the significance threshold were removed. After removing insignificant factors, the effects are recalculated. Terms were removed until only significant factors and their parents remained. Effect summaries for the other responses are given in Appendix B.2.

To further investigate the maximum temperature effect, additional simulations were conducted with temperature as the only alternating variable. When holding the other parameters as constant (3-hour holding time, 5K/min ramp rate, 53% green density, 5µm grain size for the tree, 15µm for the cube), the relationship between final density and temperature did not follow the expected pattern. The reason for using two different values for the initial grain size was that the 5µm was the standard input of the software initially used in the simulation and the 15µm grain size was later physically measured from the printing powder and was after that used as the new standard initial grain size value. Higher temperatures were expected to correlate to higher final density, but instead, the highest densities were achieved with lower maximum temperatures. The DOE model suggests that the maximum temperature and its interactions with holding time and grain size cumulatively have a statistically significant effect on the density, however, this also predicts a positive correlation. Lower temperatures creating higher-density parts are not captured in the model and defy the expectation that higher sintering temperatures should improve densification. See Figure 4.3 for a visualization of the final density vs temperature simulation results.

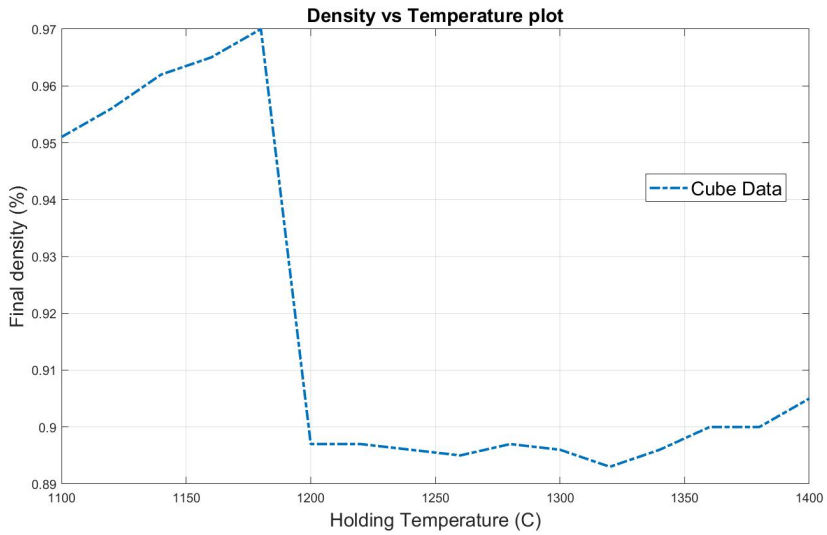

Figure 4.3: Final relative density results from varied max temperatures. The Figure represents the temperature test on the cube geometry. The grain size was set to 15µm.

Also, this analysis finds that the weight of the factors is very similar for the shrinkage in the x, y, and z-direction. While the driving factors for shrinkage are similar across the different directions, the Simufact model does not account for the sintering anisotropy in its current version.

Sagging was a measurement of interest as a type of deformation related to the sintering process. Unsupported features, like the arms of the tree, can deform due to gravity while at high temperatures. The model evaluates the grain size as the most influential factor by a wide margin. This is also the response for which holding time has its most substantial influence. This suggests that while the material parameters may be most important, the length of time that the part is kept at high temperatures also has a significant effect on the deformation. Sagging was also observed during the simulations at relatively low temperatures, even prior to densification. A graph of the impact of the holding temperature on sagging is shown in Figure 4.4.

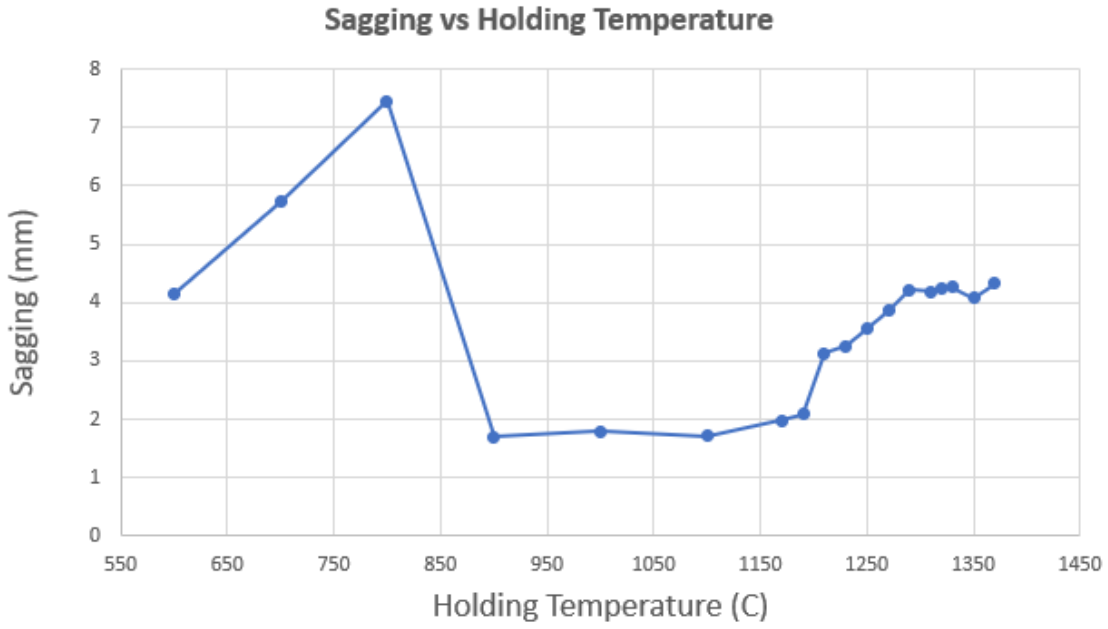

Figure 4.4: Sagging of the lowest arm in the tree geometry measured based on holding temperature during the sintering simulation.

Like with many multiple-response problems, the ideal settings will depend on how the responses are prioritized. In future applications of Simufact, a model of the software could be used to find closer to ideal settings depending on the desired outcome.

The factor weights that are displayed in Figure 4.1 indicate grain size to be of high significance for all of the responses in the model. Initially, the default setting in Simufact Additive was used: 5 µm. To improve simulation accuracy in the later stages of the project, the 316L powder used at RISE was measured. This scanning was performed five times on separate samples of the powder to ensure accurate

measurements. The averaged values are given in Table C.1 and Appendix C.1 depicts a histogram of the PSD measurements. The D50 measurement is used as the 'grain size' parameter in Simufact Additive.

D10	D50	D90	Simufact Default
8.4 µm	15.0 µm	24.7 µm	5.0 µm

Table 4.1: Measured PSD of 316L powder at RISE.

4.2 Phase 1 Geometries

Beyond the parameter study which was purely involving the simulation software, physical measurements were needed to validate the results of the software simulations. To investigate linear shrinkage and minor deformations, phase 1 geometries were used to give straightforward measurements. The primary geometry was a 10x10x10mm cube similar to what was used in Rios' work [8, 9, 10]. Beyond that, there were cubes of increasing size to see the effect of scaling geometry, cylinders, and several types of beams to investigate parts significantly larger in one dimension. The tree geometry from the parameter study was also included to be able to compare physical results to the simulated ones.

4.2.1 Simulations

All the parts were simulated in Simufact with the same material parameters and template for the sintering profile to match the conditions for the RISE sintering furnace: see Figure 3.3. The dimensions were measured using the software's measurement tool and recorded for later reference.

The simulations of the sintering curve and the final density for the tree geometry were conducted both in the Simufact additive software and in a model developed by Alberto Cabo Rios et al. [10]. This comparison was done to evaluate the results from the different models and to try and see if they have a similar approach to simulating densification over time. The results of these simulations are shown next to each other in a three-axis graph in Figure 4.5.

The most similar prediction is for the sintering profile in Figure 4.5b. Aside from this, the densification behaviors do not consistently agree. The model developed by Rios et al. accounts for phase changes and their effect on densification [10], which may contribute to the difference. Dilatometry data was available for the case shown in Figure 4.5d and when compared with the simulated data, the Simufact prediction performs poorly, greatly underestimating the densification. Equipment issues limited the amount of dilatometry data that could be gathered during the time frame of this project, so further comparisons of the Simufact densification predictions with dilatometry data are reserved for future work.

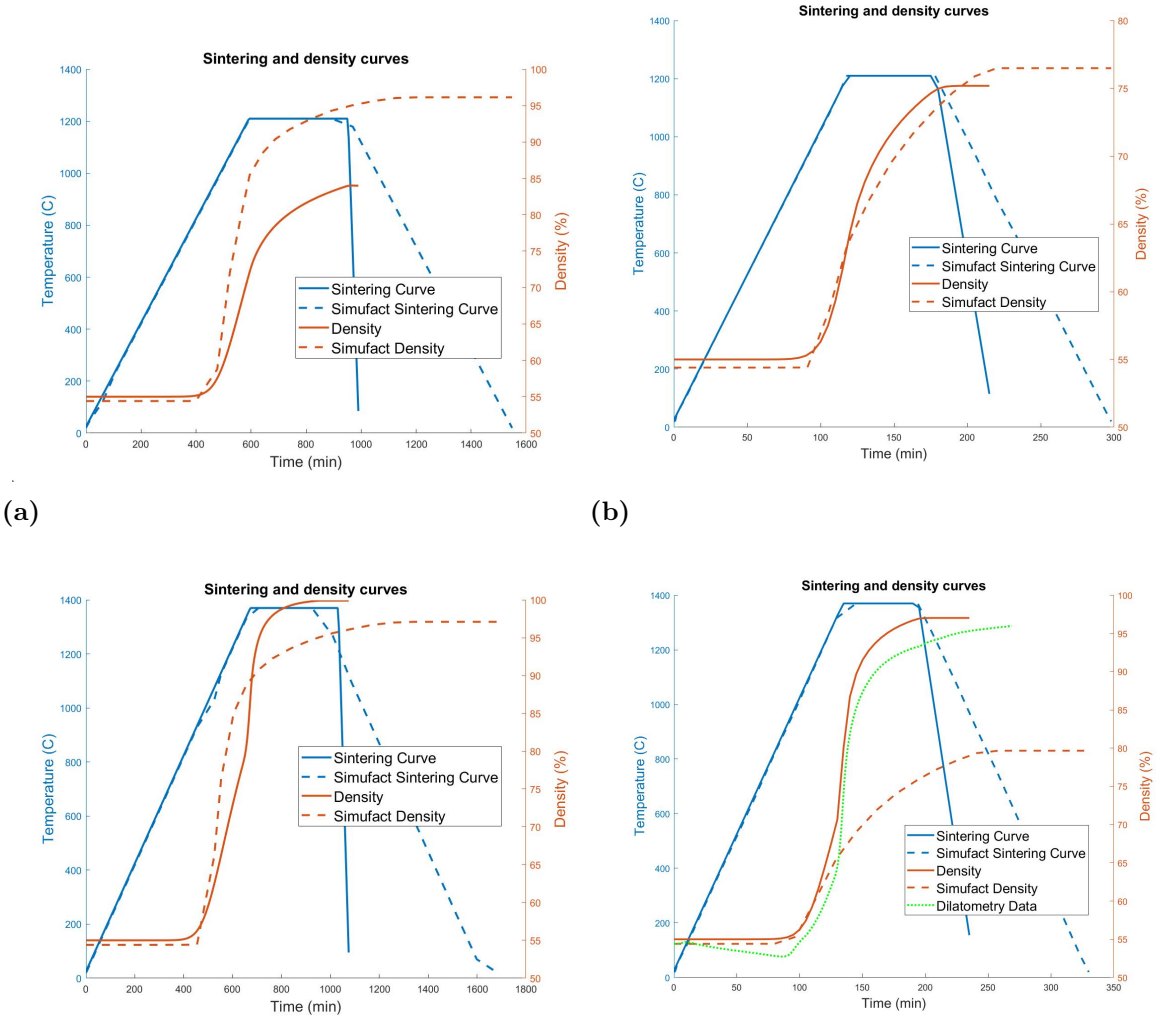

Figure 4.5: The figure shows the comparison between the simulations of the tree geometry sintering curve density development over time. The sintering profiles are as follows: Figure 4.5a maximum temperature 1210°C, ramp rate 2°C/min, 6 hour holding time; 4.5b maximum temperature 1210°C, ramp rate 10°C/min, 1 hour holding time; 4.5c maximum temperature 1370°C, ramp rate 2°C/min, 6 hour holding time; 4.5d maximum temperature 1370°C, ramp rate 2°C/min, 6 hour holding time. The dilatometry curve is not corrected for thermal expansion.

4.2.2 Sintered Part Measurements

Several copies of some of the geometries were seen in Figure 4.6 created to investigate the potential variation that could occur while printing and sintering the same geometry. One of the geometries with four copies was the tree-geometry. These prints showed small variations between each other based on weight, height, sagging, and surface quality. This was further evidenced after the sintering step of the manufacturing process based on the further variation in the sagging of the arm. One

of the arms on one of the trees even broke off during the sintering, indicating the delicate nature of the long and thin geometrical features during sintering.

Figure 4.6: Sintered phase 1 geometry processed at RISE.

The sintered cubes were investigated to measure variation in sintering shrinkage in the x, y, and z-directions. A box-chart plot of the variation in x, y, and z can be seen in Figure 4.7. Simufact did not predict significant sintering anisotropy for this geometry and underestimated the shrinkage in the z-direction (build direction).

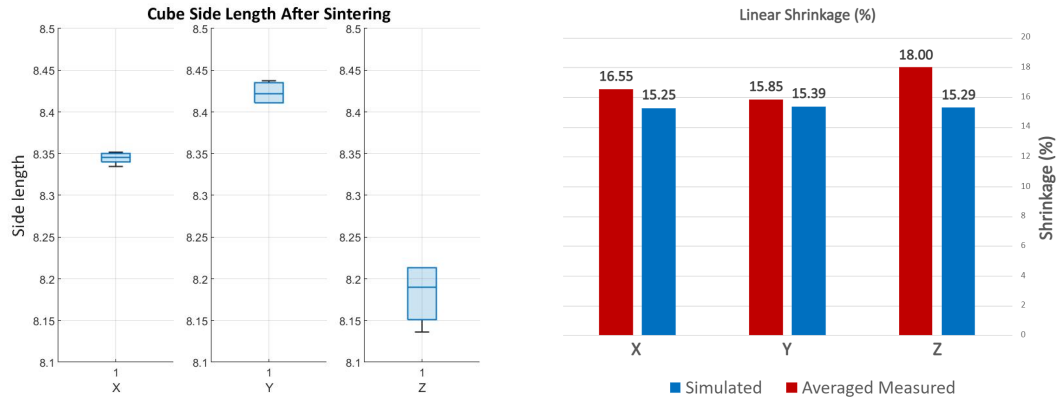

(a) **(b)**

Figure 4.7: Figure 4.7a shows a box-chart plot of the variation in sintered dimensions for the cubes in x, y, and z. The blue hollow circles in Figure 4.7a are outliers in the gathered data. The bar graph in Figure 4.7b shows the linear percentage of shrinkage in the different directions of the cube.

4.2.3 Scan Data and Model Comparisons

The GOM scanner was used to measure the printed parts before and after the sintering. These scans were done for comparisons of the printed geometry the original CAD file used by the printer. A geometrical comparison was performed and the result of the comparison was presented using a heat map. The heat map of the Tree,

after curing, can be seen in Figure 4.8, and it has a maximum deviation of 0.07 mm. Similar heat maps were created for all of the simpler geometries and they were all analyzed to ensure that a reliable print was performed without large deviations in the geometry. Volume measurements at this stage were used to estimate the green density of the parts; the average across the parts in this print job was 54.4%. A green part density distribution for the phase 1 geometry can be found in Appendix C, Figure C.3c.

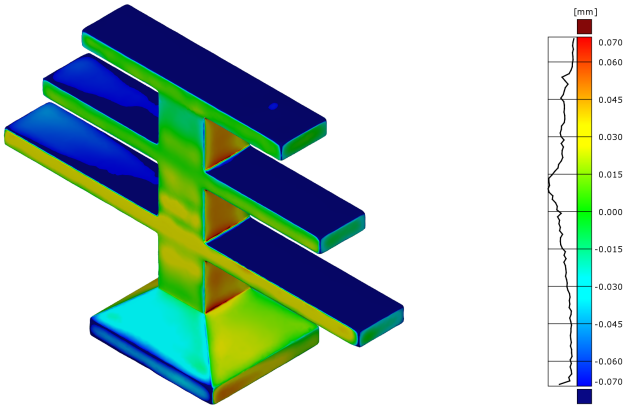

Figure 4.8: The heat map visualizes the geometrical deviation between the designed CAD geometry and the printed green part of the same geometry.

After the sintering of the parts, several scans and comparisons were performed between the various simulated sintering and the actual sintered part. The deviation between the geometries was measured and used to determine how accurate the MBJ sintering module of Simufact Additive was. The comparison was visualized and examples of these can be seen in Figure 4.9. The compiled data of Figure 4.9 are shown in Table 4.2 where it was indicated the percent of the geometry within a 0.25 mm tolerance for each of the geometries.

The initial comparison between the scanned geometry and the Simufact Additive prediction showed substantial differences, as seen in Figure 4.9a. Physical measurements from the part were used as inputs for the responses in the JMP model [25]. This JMP model could be used to determine which settings should provide the simulation results that more closely match reality. In this case, the inputs were changed from the default previously used to a higher maximum temperature (1370°C), and a longer holding time (6 hours), and the green density was updated to 55.3% based on the measurements of the green parts. This deformation simulation produced a geometry close to the physical part. The results of this model on which the JMP predictions were based are described in Section 4.1. The comparison between the JMP model prediction and the actual sintering can be seen in Figure 4.9b.

A third updated model was based on the values used in the second sensitivity analysis and the results from the geometrical comparison are shown in Figure 4.9c. This model used fixed sintering values based on measurement of the process at RISE and only applied custom material parameters for the activation energy of viscous flow and a pre-exponential constant to improve the results, 1.2E9 Pa*s and 5000

J/mol respectively. The input values along with the results of the second sensitivity analysis using the material parameters can be found in Appendix B Figure B.4 and Figure B.5.

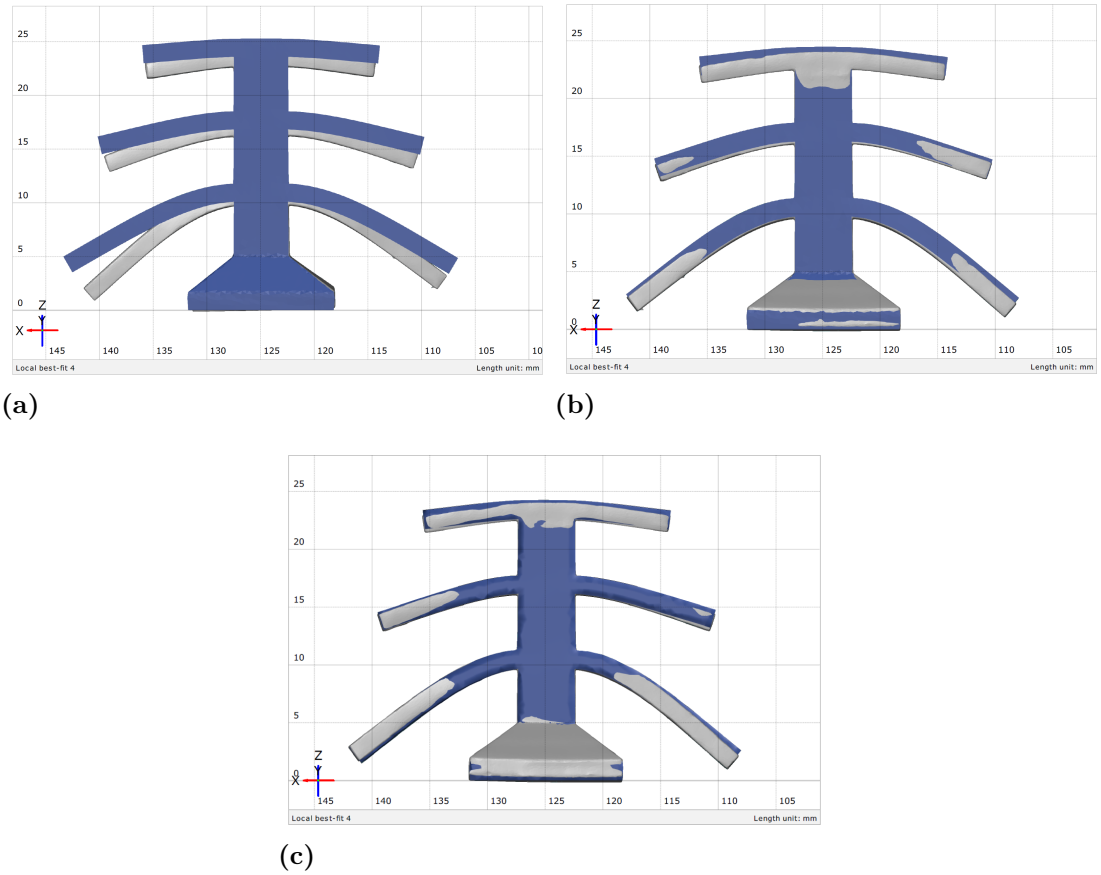

(a) (b)

(c)

Figure 4.9: A geometrical comparison of the predicted sintering deformation based on the Simufact additive model in blue, and the actual sintering deformation in grey. Figure 4.9a represents simulation parameters matching the process at RISE, Figure 4.9b represents a sintering profile from JMP, and Figure 4.9c represents custom material settings based on physical measurements and JMP recommendations.

Settings	Simufact Default	JMP Model	Custom Material
Percent within 0.25 mm	43.7%	79.3%	93%

Table 4.2: Tabulated values for the geometric deviation between the standard Simufact prediction, JMP model prediction, and the custom material model prediction. Values are taken from the geometries in Figure 4.9.

4.3 Phase 2 Geometries

For the next stage, 5 geometries were designed to include features not present in the simpler geometries. These geometries are measured for shrinkage, but the primary interest is to examine the compensation optimization tool within Simufact. The features under consideration include overhangs, bridges, arches, holes, and thin walls.

The phase 1 tree design experienced too severe deformation to be compensated, see Figure 4.10, so it was redesigned with shorter arms and fillets on some arms to investigate their effect on the arms' sagging. Sharp corners are generally avoided in designs to avoid stress concentrations, so the fillets' effect on deformation is also of interest.

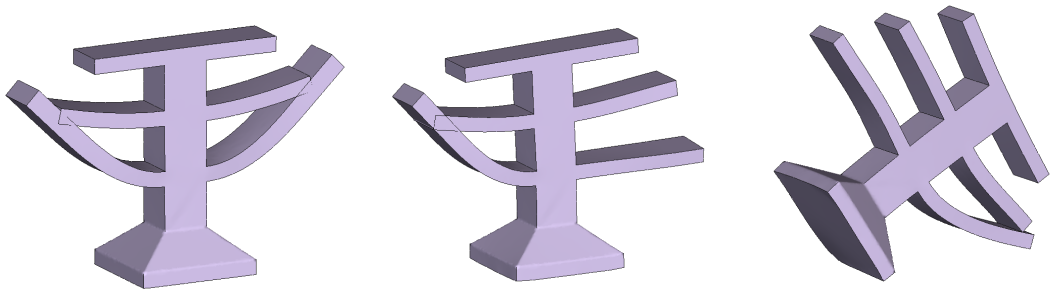

Figure 4.10: The phase 1 tree design experienced too severe deformation to be compensated. The compensation method led to self-intersecting geometry and other errors.

4.3.1 Simulation and Design Compensation

The simulations were set up similarly to before using the standard real-life sintering parameters used in the actual sintering of the physical geometries. The new setting used for this stage was the Compensation Optimization function. The function was toggled on and the acceptable deviation was set to 0.25mm. Simufact solves the FEA problem iteratively, creating compensated variants until the deviation compared to the reference geometry converges below the set value, or the process exceeds the maximum iteration count [5], in this case, 10 iterations.

From these simulations, a .stl file of the geometry can be exported from any of the variant results and used as a compensated geometry for printing. The geometries of interest are the final variant which should be sintered to the desired specification and the initial reference geometry to print using the printer manufactures recommended scaling. This allows for a controlled geometry for meaningful comparisons. This visual comparison is illustrated in Figure 4.11 and the sintered parts are shown in 4.12.

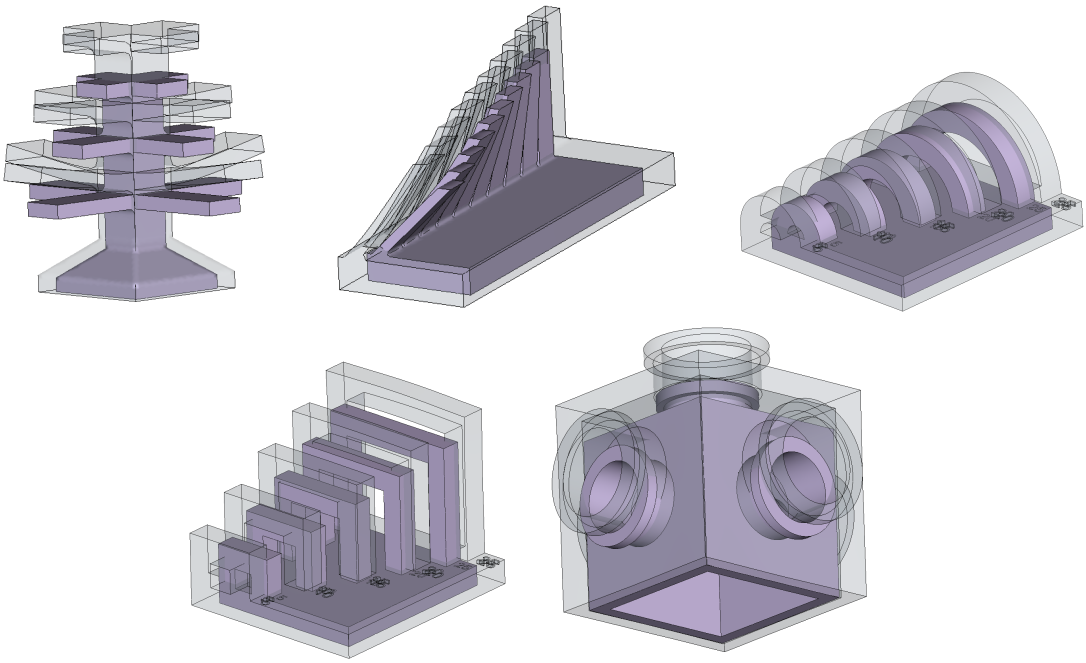

Figure 4.11: Depictions of results from the sintering compensation simulations of the phase 2 geometries with their initial solid geometry along with the compensation geometry shaded on top of them.

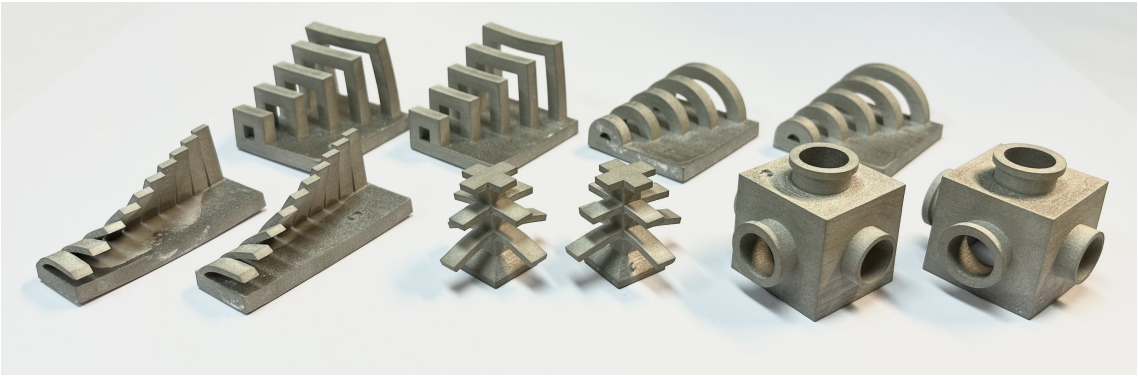

Figure 4.12: All of the sintered geometries from phase 2 of prints.

4.3.2 Scan Data

Similar to the simpler geometries, a scan of all the green parts of the second set of geometries was performed and they were also compared to the original CAD geometries to confirm a successful print job. One of these heat maps of the second tree geometry can be seen in Figure 4.13.

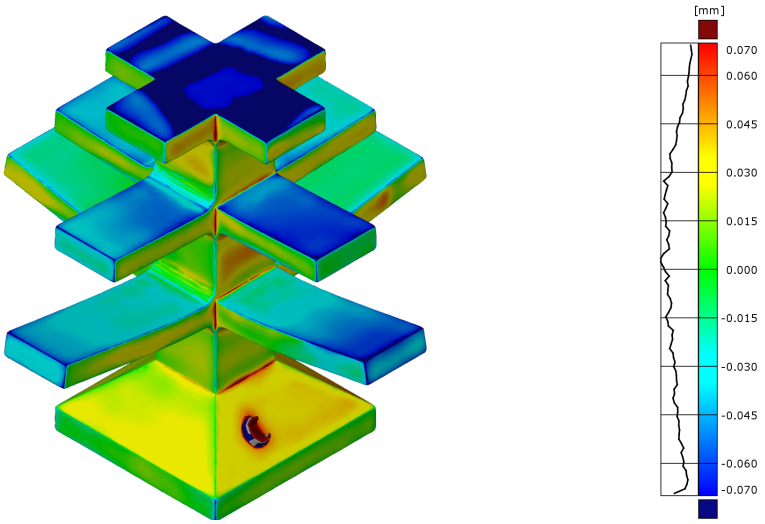

Figure 4.13: The printed geometry of the second set of geometries was scanned on compared to the created CAD files to ensure the quality of the print job. The scanning was performed on the part after it had been removed from the print bed, but before sintering. This figure shows the printed phase 2 tree compared to its CAD file.

After the sintering process was complete for the second set of geometries they were also scanned and imported into the GOM software. The scanned sintered geometry was compared to the initial shape of the part before it was compensated. This was done to see how close the compensated geometry got to the desired shape, based only on Simufact's compensation calculations.

There were two sets of prints performed for each of the second sets of geometries. One of these was compensated according to the standard Digital Metal scaling factor, which was about 1.2 in all three directions, and the other one with the results from the Simufact Additive compensation optimization simulation. Figure 4.14 visualizes tolerance analyses performed on the geometries. The green color indicates that the sintered part is within the set tolerance of 0.25 mm from the desired geometry. The yellow color means that it is within 70% - 100% of exceeding the tolerance. Finally, the red color means that the area is exceeding the set tolerance for the geometry. A compilation of the comparisons of all the sintered components is found in Table 4.3.

The geometrical comparison between the Digital Metal and Simufact Additive compensations shows that Simufact's compensated geometry stays within tolerances better in 3 of the 5 of the tested cases, as indicated by Table 4.3. The Curved and Square Arches performed the best while scaled with the Digital Metal scaling factors while the other geometries fit the CAD design better with the simulated Simufact compensation.

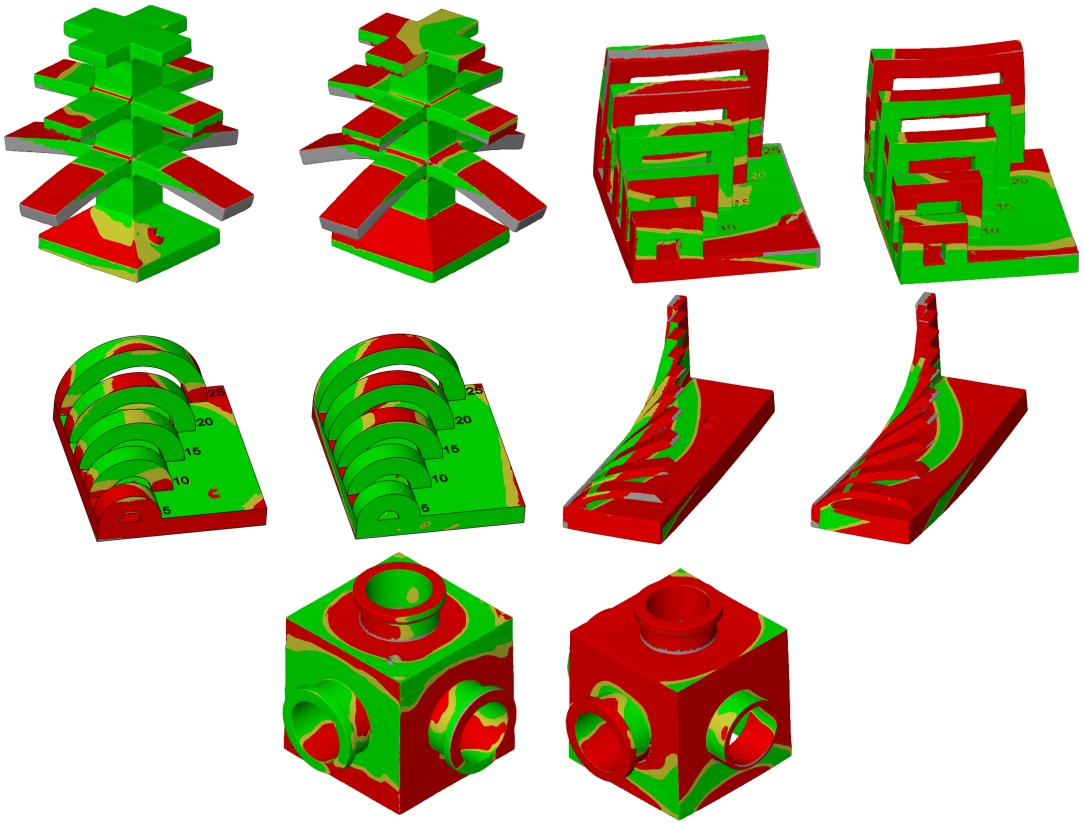

Figure 4.14: This figure depicts where the geometries are within or deviate beyond the set tolerance of 0.25. Green areas indicate the part is within tolerance, yellow indicates within the tolerance but 75% - 100% of the limit, and red exceeds the limit. The leftmost geometry in each pair is the Simufact compensated geometry and is denoted with a 'C'. The rightmost geometry in each pair is the Digital Metal scaled geometry.

Geometry	Acceptable Deviation (mm)	Simulated Deviation (mm)	Percent in Tolerance	Percent within 0.5mm
Tree	-	-	46.7%	68.5%
Tree Compensated	0.25	0.048	65.1%	83.5%
Curved Arches	-	-	87.6%	99.3%
Curved Arches Compensated	0.25	0.173	73%	89.8%
Square Arches	-	-	63%	87.0%
Square Arches Compensated	0.25	0.049	50.6%	76.9%
Angled Overhang	-	-	19.1%	45.1%
Angled Overhang Compensated	0.25	0.269*	27.9%	50.1%
Tube Cube	-	-	31.6%	92.5%
Tube Cube Compensated	0.25	0.158	58.2%	98.8%

Table 4.3: Tabulated values for geometric deviation of uncompensated and compensated geometries. * The angled overhang was unable to converge within the acceptable value, so the closest successful iteration was used.

In addition to the expected shrinkage and deformation that occurred during sintering, there was some additional warping that affected all of the geometries that included a solid base plate at the bottom. The sets of each geometry were sintered simultaneously, so it is assumed that the warping had similar effects on each geometry and the comparisons between geometries are valid. Additionally, a heavily warped section of the square arches, more precisely the largest of the arches, was excluded from both sintered components when comparing the scanned geometry to the desired CAD geometry. To do so, the surfaces of the largest arch were excluded from the scanning software prior to making the tolerance measurements.

Observation of the sagging of features on the Tree and the Angled overhang indicated that even though the Simufact compensated geometry ended up closer to the desired shape, Simufact underestimated the magnitude of the deformation. The red areas on the overhangs in both geometries presented in Figure 4.14 show this. This suggests that Simufact can predict how features are likely to occur, but not sufficiently compensate for it with the settings used in this stage of the project. The sagging of the arms in the Angled Overhang geometry was another feature that was not accounted for properly in the simulation compensation. The simulation indicated that the arms would remain mostly straight during sintering and compensated with only a minor curvature, however, the reality of the sintering showed that the arms with the larger overhang curved down substantially. As a result, half of the area of the sintered arms fell outside of the 0.25 mm tolerance.

4.4 Phase 3 Geometry

The phase 3 geometry was printed with one part using the default scaling recommended by Digital Metal and another using the compensated geometry resulting from the Simufact Additive Simulation. This set of simulations used the Compensation Optimization tool within Simufact Additive with the acceptable deviation set to 0.1 mm. A very fine mesh, ∼275,000 elements, was used to preserve the geometry's features and allow for accurate calculations.

4.4.1 Scan Data and Comparisons

The phase 3 geometry was scanned both after depowdering, as a green part, and after sintering. The scanned data were then compared to the design CAD file and the simulated sintering file respectively to get an assessment of process accuracy. After the sintering of the phase 3 geometries, they were compared in the same way that the phase 2 geometries were. The visualization of this comparison with regards to the set tolerance of 0.25 mm is shown in Figure 4.16. The tabulation of the data analyzing the geometrical variation is shown in Table 4.4.

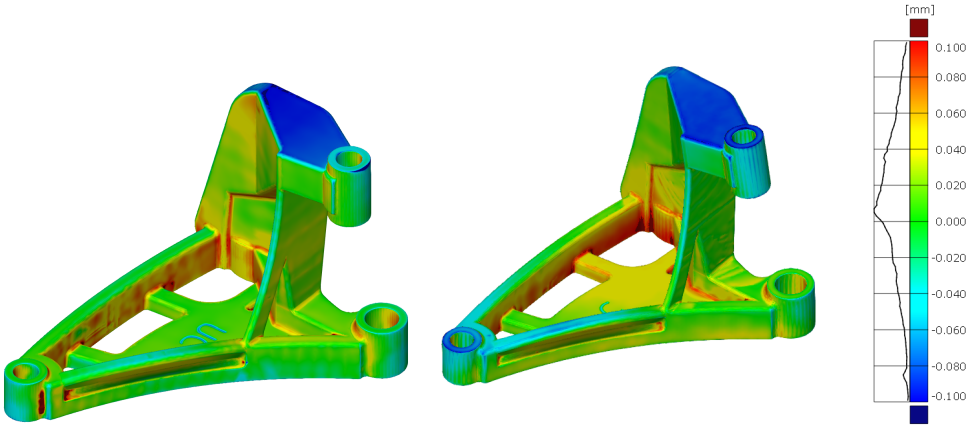

(a) **(b)**

Figure 4.15: To ensure that the print of the phase 3 geometry matched the designed geometry they were compared in GOM. The resulting heat map of the deviation can be seen in the figure above. Figure 4.15a shows the DM compensated green geometry and Figure 4.15b shows the JMP compensated green geometry.

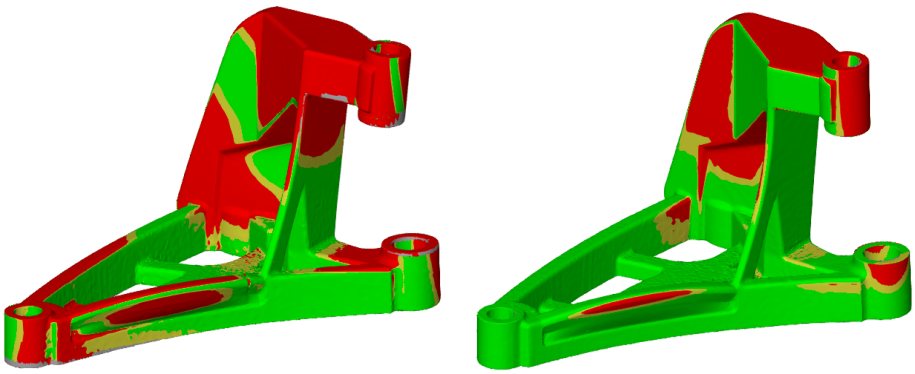

(a) **(b)**

Figure 4.16: This figure shows the geometrical comparison between the DM-scaled and JMP-scaled sintered phase 3 geometry. The green parts of the geometries are sintered to within a 0.10 mm tolerance of the predicted deformation for the desired geometries. Figure 4.16a shows the DM compensated sintered geometry and Figure 4.16b shows the JMP compensated sintered geometry.

Geometry	Acceptable Deviation (mm)	Percent in Tolerance	Percentage within 0.1 mm tolerance
Uncompensated	0.25	55.9%	25.4%
Compensated	0.25	84.2%	51.7%

Table 4.4: Tabulated values for geometric deviation of compensated phase 3 geometry.

5
Discussion

This section discusses the insights drawn from the results presented in this work. This includes comparisons of results and discussion of possible limitations associated with the project.

5.1 Phase 1 Geometries and Sensitivity Analysis

Simufact Additive does not account for sintering anisotropy in the sintering model. The differences in sintering shrinkage may be a result of numerical differences in the calculations or because of other unknown factors. This difference in shrinkage was observed in the 10mm cubes as well as in the tree geometry. For the tree geometry, scans of the green part exhibited in Figure 4.8 show that the part had deviations from the expected geometry in the z-direction prior to sintering, likely from the printing or curing stage. While minor, on a scale of 0.1mm or less, it does increase the measured anisotropy. Additionally, the sintering simulation excludes the debinding stage. While debinding contributes significantly less to shrinkage compared to sintering, it may improve results if taken into consideration.

The sensitivity analyses in JMP [25] provided insights into how to change parameters to better match simulation and physical result within the improved matches shown in Figure 4.9a, 4.9b, and 4.9c. Changing the sintering profile led to more realistic sagging behavior and more accurate shrinkage. Besides, the material model parameters were changed while keeping the sintering model as the standard RISE process to determine if the default material parameters provided were inadequate and could be determined more accurately by performing another DOE. It shows an even greater improvement over the default material setting and JMP model. This improvement is however limited to the phase 1 tree geometry and the degree to which this performance extrapolates to any other geometry. This comparison is visualized in Figure 4.9 and Table 4.2. Additionally, improving the accuracy of the simulation outputs required deviating from the sintering parameters regarding the time and temperature of the actual physical sintering process, which creates doubts about whether any given model can be applied consistently or only on a case-by-case basis. For example, the activation energy of viscous flow that yielded the best results in Simufact simulations, 5000 J/mol change from the default 20,000 J/mol, is substantially less than values reported in previous literature, including [10]. However, using values similar to previous research led to software crashes and simulation failure, with only vague indications from the software of what may have gone wrong, necessitating a heavy trial-and-error approach. Preferably, the error messages could

be updated with more specific causes of the crash, or potential methods to address the cause of the error.

The impact of the holding temperature on simulated densification and deformation of the geometry has contradicted established findings from previous research.
The low temperature should correspond to low density with an increasing density corresponding to an increase in temperature. This was not observed in simulations using either the tree or the 10mm cube geometries. Both geometries were investigated because the sagging of the arms in the tree could affect the final density of the part in the simulation and as the cube has no such features it would be immune to this effect. Further investigations will need to be done to isolate the particular parameters that are causing this strange behavior. Significant shifts in the simulated behavior were observed at 800°C and 1200°C, and densification and sagging can be seen in the simulations at low temperatures at which such phenomena are not expected.

5.2 Design Compensation

Simufact Additive's Compensation Optimization feature was used on the second set of geometries to determine if the geometry predicted by this feature could provide more accurate sintering geometries than Digital Metal's standard scaling-only compensation. The results of this comparison were presented in Table 4.3 and it showed that 3 of the 5 sintered geometries conformed more accurately to the defined tolerances when pre-deformed by Simufact's Compensation Optimization tool. Simufact failed to outperform the scaling-only approach with components with arches as the dominant feature. The reason for this is unclear but it could be that the self-supporting nature of these features is ill-accounted for in the Simufact software or while adequately accounted for with scaling.

The geometries were intentionally designed to have features that deformed significantly to test the limitations of the compensation tool in the software. Three of these features also contained a base plate that distorted rather substantially during the sintering and this could also have been a contributing factor to the poor prediction of the software as the geometry did not end up as intended. One interesting area where Simufact provided an improvement in geometry was in the sagging on the top and in the middle of some geometries. These improvements can be seen in the Tube Cube, the updated Tree, and arches where the top surfaces show a higher amount of area within tolerance than the DM scaling geometry. In this case, Simufact's pre-deformation of these areas counteract the expected gravitational sagging during sintering. The compensation is an improvement but as mentioned before with the arms in the tree, it can be further improved, as indicated by the still red areas on some of the improved geometries seen in Figure 4.14.

The simulation approach for the phase 3 geometry used a more customized set of sintering inputs relating to holding time and temperature, based on additional physical measurements and insights from the sensitivity analysis. These calibration efforts led to improvements in the results with the compensated geometry conforming

to tolerances significantly better, compared to an uncompensated geometry. The top surface in the green body showed the most deviation which may have contributed to the top surface not meeting tolerances in the sintered part. The calibration efforts were extrapolated from insights from the basic tree geometry, but the degree to which this can be applied to other geometries comprehensively requires further investigation.

5.3 Limitations

Due to the limited time frame of the work and the lead times associated with creating a physical sample, many of the tasks in this project were addressed concurrently. As such, the compensation simulations for the printed geometries were run with default settings or slightly altered settings for the material and process parameters, even while other parameters were under investigation. The results are reflective of this, but it is unclear how further customizing the model to reflect the printing and sintering process at RISE would affect the results. Additionally, results of the phase 2 geometry were received after the complex geometry was simulated and printed, so while the findings are reported in the results time restrictions prevented them from being integrated into improving the final simulations.

The sensitivity DOE did not include all parameters that are available to change in the Simufact Additive material library for sintering. Rather values that were known or easily measurable were the focus; these also being parameters that there would be some control to change to see to what extent changing would affect results according to Simufact (e.g. sieving powder to a finer D50). Later stages investigated other material parameters and their effect on the simulations. The material model to a large extent determines the results of the simulation. Ideally, an accurate material model would allow for accurate results across multiple simulations and a variety of geometries while keeping the process parameters constant and representative of the real process. This project has shown that the simulation results be made to match physical parts by changing the material model and/or the process parameters. It remains to be seen, however, how well these changes translate to other geometries, or if the parameters would need to be changed further to yield similarly accurate results.

6
Conclusions and Future Work

While the default material model parameters applied to the actual sintering profile did not yield accurate results, calibration efforts showed improvement. The default model does not include the anisotropy of the sintering shrinkage in phase 1 geometries and did not account for the magnitude of the deformation during sintering with consistent accuracy. Changing the material model parameters and simulated sintering profile for the geometries considered in this work resulted in simulation predictions that matched more closely with the physical sintered parts, reaching as high as 93% of surfaces within 0.25mm of the ideal in the best case. While ideal material settings for use in the simulation to give consistent and accurate results can likely be easily improved and updated, at this time there is no established methodology to determine the values for a given process. The lack of a clear method to reliably fit the Simufact Additive simulations to an individual process and the lack of feedback provided by the software poses an obstacle for the users of the software and is a potential area for improvement.

Simufact Additive's Compensation Optimization tool exhibited inconsistent success in compensating the geometries to fulfill the defined tolerances. Geometrical features, such as long overhangs, conformed to tolerances better after simulation but still deviated significantly from the desired geometry. This suggests that some features may not be appropriate to solely address using pre-deformed geometry, and other methods such as sintering support, part orientation, or redesigning the geometry should be considered. To that end, Simufact Additive may not be a cure-all solution to the issue but one of several tools to identify and address design flaws and other DfAM obstacles.

Suggestions for future work:

- Develop a methodology for fitting the model to individual processes to account for the variation in the process parameter, equipment, material, etc.
- Investigate the extent to which a custom model can be applied to a variety of processes and geometries and how the results are affected accordingly.
- Investigate how sintering setters or supports can be used in tandem with Simufact Additive to improve design compensation efforts.

Bibliography

[1] "Iso/astm 52900:2021 additive manufacturing — general principles — fundamentals and vocabulary," https://www.iso.org/obp/ui/, accessed: 2023-4-28.

[2] M. Li, W. Du, A. Elwany, Z. Pei, and C. Ma, "Binder jetting additive manufacturing of metals: A literature review," 06 2019.

[3] S. Sadeghi Borujeni, A. Shad, K. Abburi Venkata, N. Günther, and V. Ploshikhin, "Numerical simulation of shrinkage and deformation during sintering in metal binder jetting with experimental validation," *Materials Design*, vol. 216, p. 110490, 2022. [Online]. Available: https://www.sciencedirect.com/science/article/pii/S0264127522001113

[4] The 17 goals. [Online]. Available: https://sdgs.un.org/goals

[5] H. AB, 2022. [Online]. Available: https://www.simufact.com/application-metal-binder-jetting.html

[6] Google trend for metal additive manufacturing. [Online]. Available: https://trends.google.com/trends/explore?date=all&q=metal%20additive%20manufacturing

[7] C. C. Amy Elliott, *Additive manufacturing processes*, 2020, vol. 24, ch. Binder Jetting and Sintering in Additive Manufacturing. [Online]. Available: https://doi.org/10.31399/asm.hb.v24.a0006569

[8] A. Cabo Rios, E. Hryha, E. Olevsky, and P. Harlin, "Sintering anisotropy of binder jetted 316l stainless steel: part i – sintering anisotropy," *Powder Metallurgy*, vol. 65, pp. 1–10, 12 2021.

[9] ——, "Sintering anisotropy of binder jetted 316l stainless steel: part ii – microstructure evolution during sintering," *Powder Metallurgy*, vol. 65, pp. 1–13, 01 2022.

[10] A. Cabo Rios, E. Olevsky, E. Hryha, M. Persson, and R. Bordia, "Analytical models for initial and intermediate stages of sintering of additively manufactured stainless steel," vol. 249, p. 118822, 03 2023.

[11] What is binder jetting 3d printing? [Online]. Available: https://www.hubs.com/knowledge-base/introduction-binder-jetting-3d-printing/#pros-cons

[12] *Additive Manufacturing Process Classification, Applications, Trends, Opportunities, and Challenges*. John Wiley Sons, Ltd, 2021, ch. 1, pp. 1–30. [Online]. Available: https://onlinelibrary.wiley.com/doi/abs/10.1002/9781119210801.ch1

[13] M. Khalid and Q. Peng, "Sustainability and environmental impact of additive manufacturing: A literature review," *Computer-Aided Design and Applications*, vol. 18, pp. 1210–1232, 02 2021.

[14] S. Bafaluy Ojea, J. Torrents-Barrena, M. T. Pérez-Prado, R. Muñoz Moreno, and F. Sket, "Binder jet green parts microstructure: advanced quantitative analysis," *Journal of materials research and technology*, vol. 23, p. 3974–3986, 2023. [Online]. Available: https://www.sciencedirect.com/science/article/pii/S2238785423002831

[15] L. Sun, Y.-H. Kim, D. d.-W. Kim, and P. Kwon, "Densification and properties of 420 stainless steel produced by three-dimensional printing with addition of si3n4 powder," *Journal of manufacturing science and engineering*, vol. 131, no. 6, p. 061001, 2009. [Online]. Available: https://asmedigitalcollection.asme.org/manufacturingscience/article-abstract/131/6/061001/450500/Densification-and-Properties-of-420-Stainless?redirectedFrom=fulltext

[16] *Basics of Metal Additive Manufacturing*. John Wiley Sons, Ltd, 2021, ch. 2, pp. 31–90. [Online]. Available: https://onlinelibrary.wiley.com/doi/abs/10.1002/9781119210801.ch2

[17] Y. Wang and Y. Zhao, "Investigation of sintering shrinkage in binder jetting additive manufacturing process," *Procedia Manufacturing*, vol. 10, pp. 779–790, 12 2017.

[18] R. M. German, "Coarsening in sintering: Grain shape distribution, grain size distribution, and grain growth kinetics in solid-pore systems," *Critical Reviews in Solid State and Materials Sciences*, vol. 35, no. 4, pp. 263–305, 2010. [Online]. Available: https://doi.org/10.1080/10408436.2010.525197

[19] "Sintering trajectories: Description on how density, surface area, and grain size change," *JOM*, vol. 68, 01 2016.

[20] "Simufact Additive: Accelerating the metal Binder Jetting workflow with sintering simulation, journal =."

[21] E. Stevens, S. Schloder, E. Bono, D. Schmidt, and M. Chmielus, "Density variation in binder jetting 3d-printed and sintered ti-6al-4v," *Additive manufacturing*, vol. 22, p. 746–752, 2018. [Online]. Available: https://www.sciencedirect.com/science/article/pii/S221486041830232X

[22] Y. Bai, G. Wagner, and C. B. Williams, "Effect of particle size distribution on powder packing and sintering in binder jetting additive manufacturing of metals," *Journal of manufacturing science and engineering*, vol. 139, no. 8, p. 081019, 2017. [Online]. Available: https://asmedigitalcollection.asme.org/manufacturingscience/article/139/8/081019/376387/Effect-of-Particle-Size-Distribution-on-Powder

[23] ——, "Effect of bimodal powder mixture on powder packing density and sintered density in binder jetting of metals." [Online]. Available: http://utw10945.utweb.utexas.edu/sites/default/files/2015/2015-62-Bai.pdf

[24] H. AB, "Simufact additive tutorial," Tutorial provided within licensed Simufact Additive software, 2022.

[25] JMP, 2023. [Online]. Available: https://www.jmp.com/en_us/software/data-analysis-software.html

Appendix A. Printer Settings

Name

PB4, 2PH, 316L, Dark 8/8/3, Lissel long, Normal, MultiOffsetFull

Description

Suitable for larger sized components, Low print speed, high surface finish

Print box type	PB4
Number of printheads	2
Powder material	316L
Binder type	C20
Add print walls	Yes
Print wall thickness	60
Shell thickness	1 pixels
Shell raster type	Dark 8
Inner shell thickness	0 pixels
Inner shell raster type	Dark 8
Body raster type	Dark 3
Resolution	1200 dpi
Print layer thickness	42.000 µm
Stripe set	PB4 2-PH Lissel Long
Offset type	Multi
Multi offset set	Multi 1
Number of base layers	50
Cleaning interval	5
Powder magazine temperature	70.000 °C
Powder applicator temperature	70.000 °C
Print box temperature	80.000 °C
Number of print speed 1 layers	0
Print speed 2	200 mm/s
Print speed 1	50 mm/s
Powder applicator speed	30
Powder application actuators pos dir	1 2 3 4 5 6 7 8 9 10 (all checked)
Powder application actuators neg dir	1 2 3 4 5 6 7 8 9 10 (all unchecked)
Enable powder bed camera	After print
Enable print head inspection	Disable
Time from print end to powder application	0.000 s
Recipe type	DM Standard

Figure A.1: Settings used when printing with the DM P2500.

Appendix B. DOE Data

	Max Temp	Holding Time	Initial Dens	Ramp Rate	Grain Size	Final Density	Deviation X	Deviation Y	Deviation Z	Sagging
1	1210	1	50	10	5	0,862	1,202	1,198	1,202	2,646
2	1370	3,5	65	10	5	0,939	1,134	1,128	1,135	4,475
3	1370	1	65	2	5	0,99	1,161	1,152	1,165	3,747
4	1370	1	50	6	45	0,712	1,131	1,122	1,131	7,568
5	1210	1	65	10	25	0,784	1,067	1,063	1,067	3,644
6	1370	6	50	10	5	0,939	1,24	1,229	1,241	5,624
7	1210	6	65	6	5	0,972	1,148	1,14	1,149	4,309
8	1290	1	50	2	5	0,99	1,263	1,254	1,267	3,1
9	1370	1	57,5	10	45	0,717	1,08	1,075	1,08	5,453
10	1370	6	50	2	25	0,942	1,247	1,225	1,251	10,06
11	1210	1	65	2	45	0,852	1,102	1,09	1,103	9,543
12	1290	3,5	57,5	6	25	0,855	1,147	1,137	1,148	7,231
13	1210	6	50	10	45	0,789	1,173	1,16	1,173	9,097
14	1290	6	65	10	45	0,864	1,106	1,094	1,107	8,593
15	1210	6	57,5	2	5	0,99	1,209	1,198	1,214	4,477
16	1370	6	65	2	45	0,933	1,14	1,118	1,142	11,01
17	1210	3,5	50	2	45	0,839	1,2	1,18	1,2	10,5
18	1370	6	65	10	45	0,872	1,11	1,097	1,111	8,992
19	1290	6	50	2	45	0,886	1,223	1,201	1,225	10,24
20	1290	1	65	2	5	0,99	1,159	1,151	1,163	3,303
21	1290	6	50	10	5	0,924	1,233	1,222	1,234	5,758
22	1210	6	65	10	45	0,852	1,1	1,091	1,101	8,174
23	1290	1	50	10	45	0,65	1,095	1,089	1,095	5,677
24	1210	1	50	2	5	0,99	1,262	1,254	1,265	2,831
25	1370	1	50	2	5	0,99	1,263	1,253	1,267	3,25
26	1320	3	53	5	5	0,963	1,224	1,217	1,226	4,247

Figure B.1: Full data table for DOE investigating process parameters.

Source	Logworth	PValue
Grain Size(5,45)	13.381	0.00000
Ramp Rate(2,10)	10.514	0.00000
Holding Time(1,6)	9.080	0.00000
Initial Dens(50,65)	4.434	0.00004
Grain Size*Holding Time	4.092	0.00008
Grain Size*Initial Dens	2.945	0.00114
Ramp Rate*Holding Time	2.415	0.00384

(a)

Source	Logworth	PValue
Initial Dens(50,65)	14.320	0.00000
Grain Size(5,45)	11.596	0.00000
Ramp Rate(2,10)	9.811	0.00000
Holding Time(1,6)	8.577	0.00000
Grain Size*Holding Time	3.980	0.00010
Initial Dens*Grain Size	2.736	0.00183
Ramp Rate*Holding Time	2.144	0.00717

(b)

Source	Logworth	PValue
Initial Dens(50,65)	13.676	0.00000
Grain Size(5,45)	12.075	0.00000
Ramp Rate(2,10)	8.073	0.00000
Holding Time(1,6)	6.705	0.00000
Grain Size*Holding Time	4.051	0.00009
Initial Dens*Grain Size	3.073	0.00085

(c)

Source	Logworth	PValue
Initial Dens(50,65)	14.428	0.00000
Grain Size(5,45)	11.901	0.00000
Ramp Rate(2,10)	10.257	0.00000
Holding Time(1,6)	8.791	0.00000
Grain Size*Holding Time	4.186	0.00007
Initial Dens*Grain Size	2.865	0.00136
Ramp Rate*Holding Time	2.197	0.00635

(d)

Source	Logworth	PValue
Grain Size(5,45)	15.194	0.00000
Grain Size*Ramp Rate	7.562	0.00000
Holding Time(1,6)	7.445	0.00000
Ramp Rate(2,10)	5.782	0.00000 ^
Grain Size*Grain Size*Holding Time	4.251	0.00006
Holding Time*Ramp Rate	4.005	0.00010
Grain Size*Grain Size	3.113	0.00077 ^
Grain Size*Holding Time	0.272	0.53404 ^

Remove Add Edit Undo FDR ('^' denotes effects with containing effects above them)

(e)

Figure B.2: Significant factor weights for (a) final relative density, (b) shrinkage in x, (c) shrinkage in y, (d) shrinkage in z, (e) sagging of the longest arms

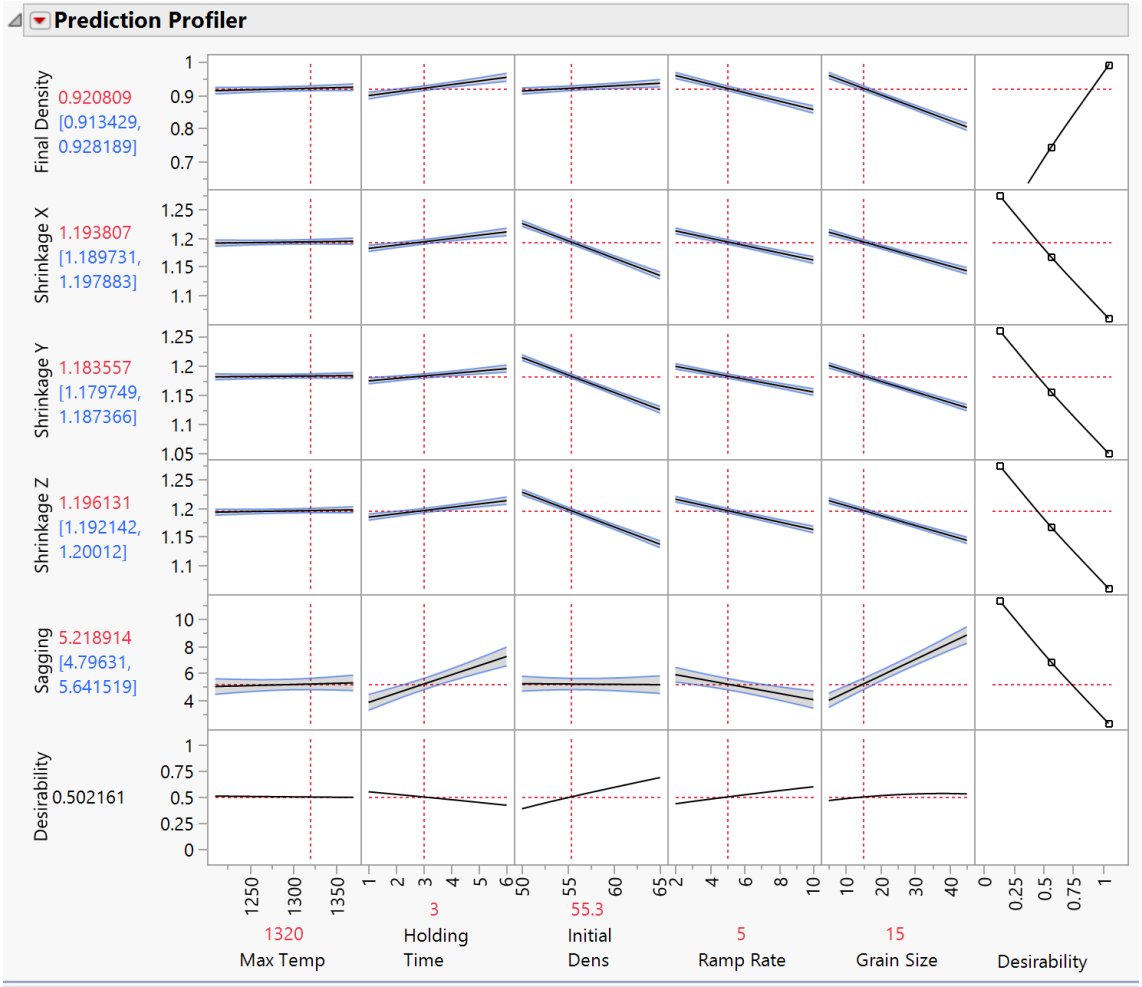

Figure B.3: JMP generated prediction profiler used to estimate responses based on the factor weights and inputs.

	Activation Energy	PreEx Constant	Final Density	X	Y	Z	Sagging
1	2500	3	99	4.634	4.843	21.97	8.63
2	2500	6	99	4.8	4.95	23.32	9.537
3	2500	9	99	4.86	4.925	23.82	9.858
4	16250	3	99	4.866	4.906	24.01	8.452
5	16250	6	96.9	4.915	4.979	24.51	7.365
6	16250	9	92.6	4.998	5.043	24.94	7.204
7	30000	3	92.2	5.008	5.049	25	6.52
8	30000	6	80.5	5.245	5.278	26.23	5.246
9	30000	9	74.5	5.387	5.411	26.94	4.193
10	20000	7.8	90.1	5.047	5.089	25.21	6.691
11	10000	3	99	4.747	4.911	23.39	9.624
12	10000	6	99	4.865	4.944	24.12	7.942
13	10000	9	97.6	4.911	4.964	24.41	8.03
14	8175	8	99	4.898	4.929	24.19	7.801
15	7350	8.5	99	4.898	4.93	24.23	8.055
16	12000	6	99	4.901	4.926	24.23	6.977
17	6500	9	99	4.875	4.952	24.16	8.188
18	10000	7	99	4.877	4.952	24.22	7.886
19	14200	4.84	99	4.877	4.948	24.23	6.961
20	5000	12	98.6	4.881	4.964	24.25	8.489
21	30000	1	99	4.851	4.934	24.09	8.165
22	4000	12	98.9	4.875	4.959	24.18	8.636
23	4000	12.5	99.8	4.871	4.87	24.21	9.658

Figure B.4: Full data table for DOE investigating other material parameters.

Source	Logworth	PValue
Activation Energy(2500,30000)	12.191	0.00000
PreEx Constant(3,9)	10.686	0.00000
PreEx Constant*Activation Energy	5.828	0.00000

Figure B.5: Effect summary of the activation energy and pre-exponential constant.

Appendix C. Additional Physical Measurement Data

Element	Fe	Cr	Ni	Mo	C
Weight %	Balance	17.0	11	2.2	0.015

Table C.1: Chemical composition of 316L powder at RISE.

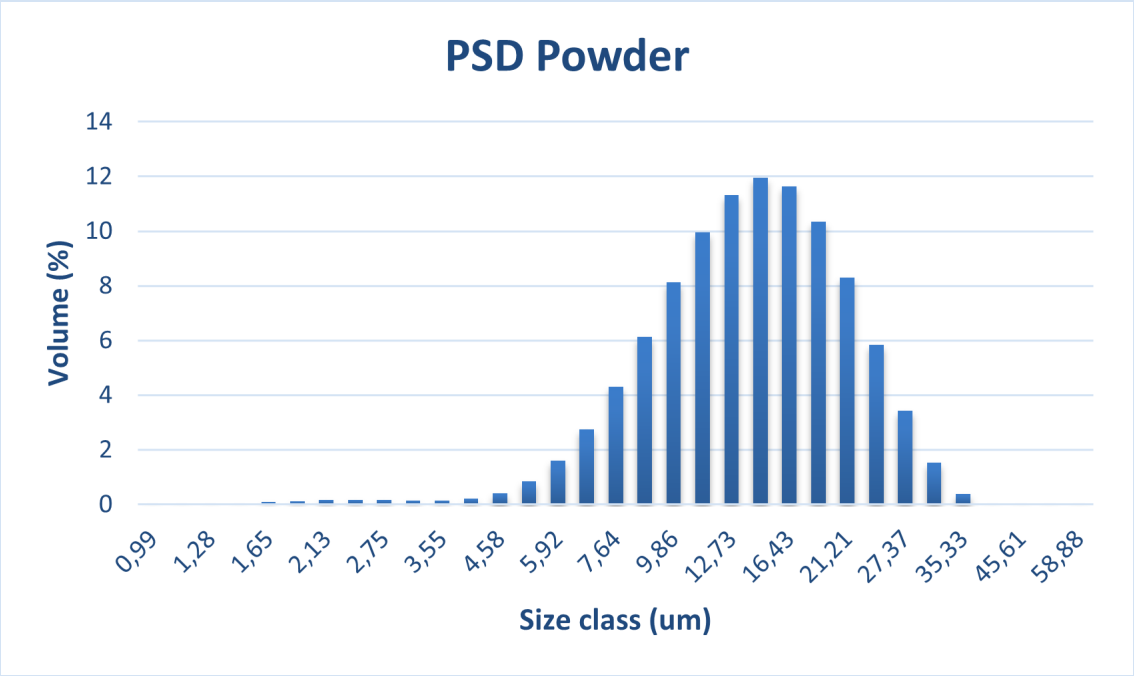

Figure C.1: A histogram of the PSD of the 316L powder that was used for the printing of the components.

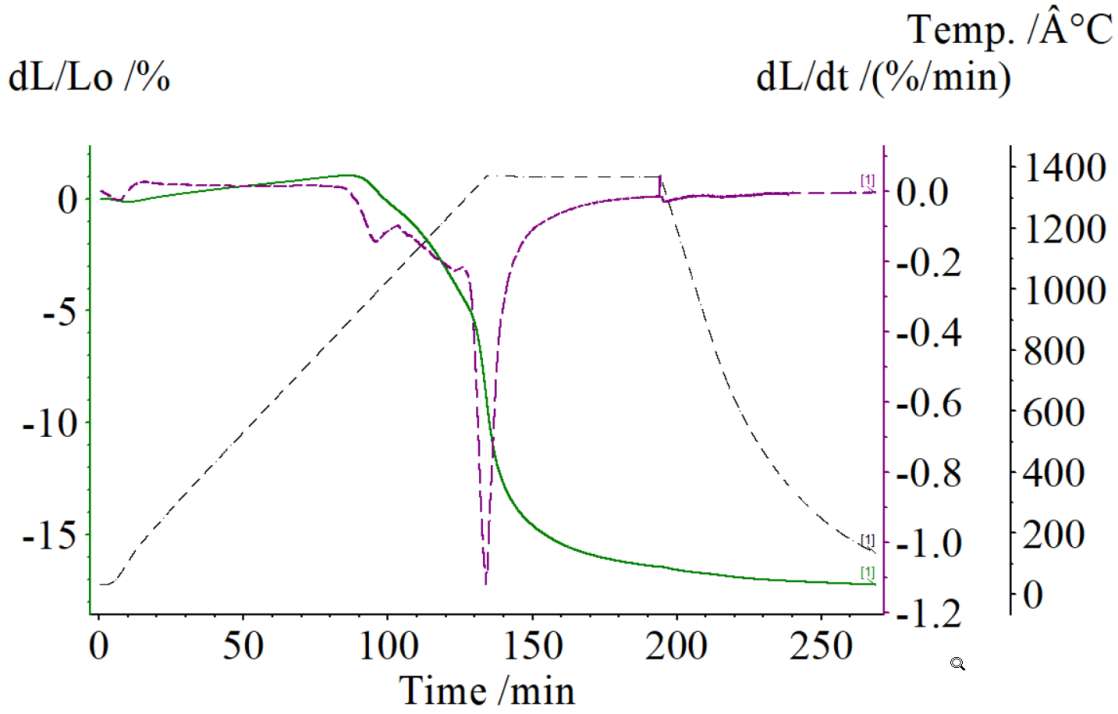

Figure C.2: Dilatometry measurements gather by Ablerto Cabo Rios used for comparison with simulated values.

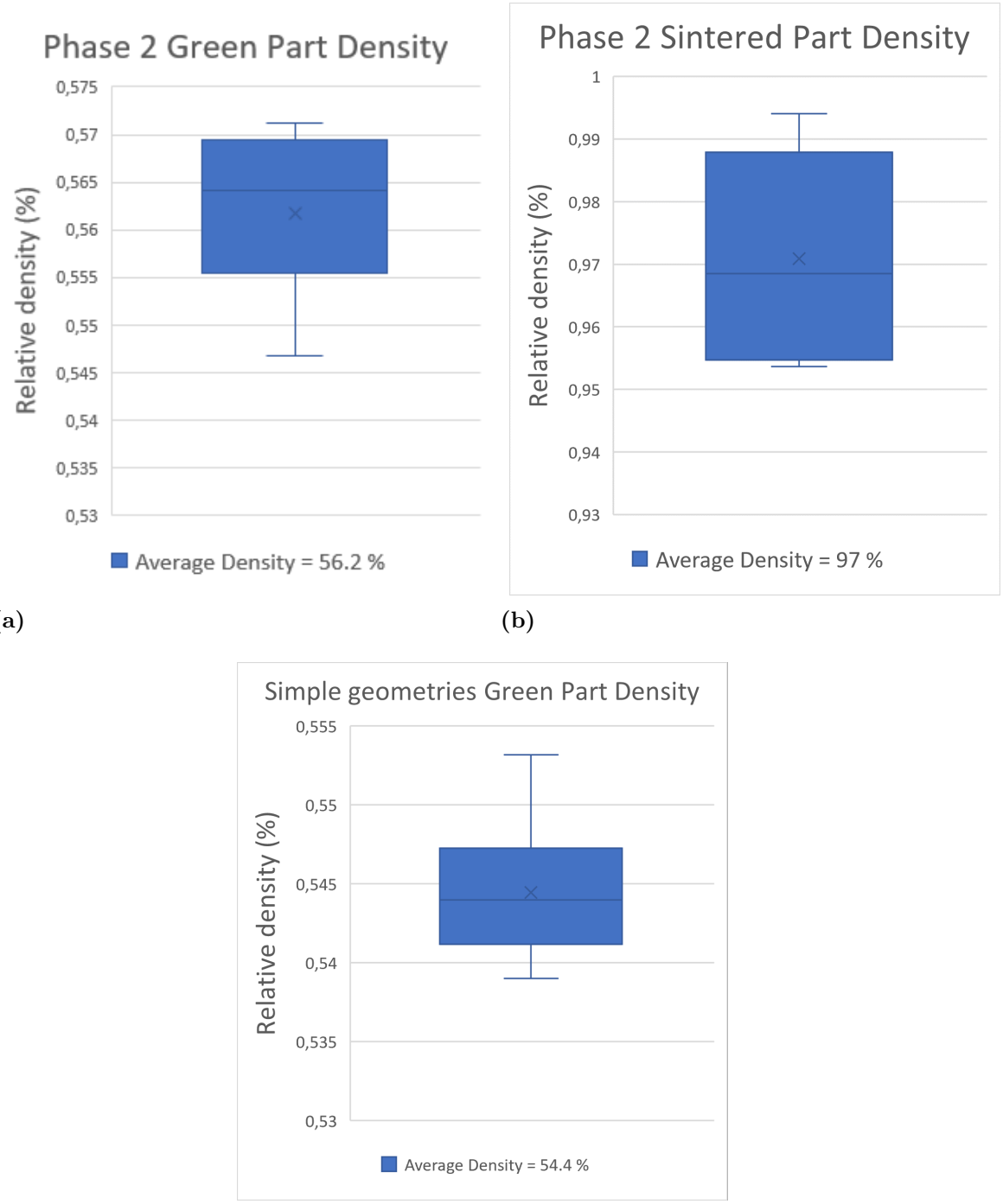

(a) **(b)**

(c)

Figure C.3: A compilation of the measured green part and sintered part density for some printed geometries. Figure C.3a shows the green part density distribution for the second phase of the geometries and Figure C.3b shows the sintered part density distribution for the same parts. Figure C.3c illustrates the green part density distribution for the simple geometries.

Department of Industrial and Materials Science
CHALMERS UNIVERSITY OF TECHNOLOGY
Gothenburg, Sweden
www.chalmers.se

CHALMERS
UNIVERSITY OF TECHNOLOGY